UC Santa Barbara

UC Santa Barbara Electronic Theses and Dissertations

Title

Organic Preservation of Vase-Shaped Microfossils from the Late Tonian Chuar Group, Grand Canyon, Arizona

Permalink

https://escholarship.org/uc/item/97k2z576

Author

Tingle, Kelly Elizabeth

Publication Date

2021

Peer reviewed|Thesis/dissertation

eScholarship.org Powered by the California Digital Library
University of California

UNIVERSITY OF CALIFORNIA

Santa Barbara

Organic Preservation of Vase-Shaped Microfossils from the Late Tonian Chuar Group, Grand Canyon, Arizona

A Thesis submitted in partial satisfaction of the

requirements for the degree Master of Science

in Marine Science

by

Kelly Elizabeth Tingle

Committee in charge:

Professor Susannah Porter, Chair

Professor Andrew Czaja, University of Cincinnati

Professor Morgan Raven

Professor Bruce Tiffney

September 2021

The thesis of Kelly Elizabeth Tingle is approved.

Andrew Czaja

Morgan Raven

Bruce Tiffney

Susannah Porter, Committee Chair

July 2021

Organic Preservation of Vase-Shaped Microfossils from the Late Tonian Chuar Group,

Grand Canyon, Arizona

Copyright © 2021

by

Kelly Elizabeth Tingle

ACKNOWLEDGEMENTS

I acknowledge the Kaibab tribe of the Southern Paiute people and the Chumash people, the original stewards of the lands on which the samples were collected that were used in this study, and the lands on which I completed this research. I thank Bonnie Bloeser and Robert Horodyski for providing the samples studied in this research. I would like to thank my advisor, Dr. Susannah Porter, for her kindness, wisdom, enthusiasm, and guidance. I would like to thank my committee members, Dr. Andrew Czaja, for assistance with Raman spectroscopy and data analysis and presentation, and Drs. Morgan Raven and Bruce Tiffney, for their guidance and feedback on earlier drafts. Gareth Seward assisted me with SEM and EPMA analysis and data presentation, and Lee Sharpnack helped to prepare my samples. My research benefitted from discussion with Heda Agić, Lena Capece, Alex Johnson, John Moore, Leigh Anne Riedman, and Tina Woltz. This work was funded by an IGPMS Summer Fellowship, a student research award from the Clay Minerals Society, and funding awarded to Susannah Porter from the UCSB Academic Senate.

ABSTRACT

Organic Preservation of Vase-Shaped Microfossils from the Late Tonian Chuar Group, Grand Canyon, Arizona

by

Kelly Elizabeth Tingle

Vase-shaped microfossils (VSMs) are a group of early eukaryotic microfossils found globally in middle Neoproterozoic (800–730 Ma) marine strata and are interpreted as the earliest evidence for testate (shell-forming) amoebozoans. VSM tests are hypothesized to have been originally organic in life, and VSMs are occasionally reported preserved with carbonaceous tests. However, many of these reports are not confirmed. Bloeser (1985) reported carbonaceous VSMs from shales of the Walcott Member, Chuar Group, Grand Canyon, Arizona, USA, but Porter and Knoll (2000) suggested these specimens were organic-coated siliceous casts after analyzing stratigraphically equivalent VSM material. The goal of this study was to re-examine the microfossils reported by Bloeser (1985) and determine if these VSMs were actually preserved with organic tests. We identified VSMs from two samples of black shales from the Walcott Member in transmitted light microscopy and used scanning electron microscopy (SEM) to image VSMs. Energy dispersive x-ray spectroscopy was used to gain a qualitative understanding of VSM composition and wavelength dispersive x-ray spectroscopy was used to assess elemental spatial variation at a finer resolution. Raman spectroscopy was used to identify mineral components and to

compare the thermal maturity of carbonaceous material within the samples. Of the VSM tests sampled, 29 possess carbonaceous tests and 37 have tests that are either partially or completely replaced by pyrite and an iron-phosphate mineral, possibly vivianite. Within some tests, the pyrite has been irregularly oxidized to jarosite. Carbonaceous material is found within the tests of all VSMs from both samples, which we suspect may be bitumen generated during the Phanerozoic (Cretaceous or later) within the Walcott Shales. Based on our observations and chemical analysis, we conclude that the VSMs are preserved with original organic test material, and speculate that sulfurization may have promoted organic preservation, consistent with observations of organic VSMs associated with sulfur, high total organic carbon content, and low concentrations of iron.

TABLE OF CONTENTS

LIST OF FIGURES

I. Introduction

Vase-shaped microfossils (VSMs) are a group of early eukaryotic microfossils found globally in late Tonian (800–730 Ma) marine strata. VSMs are interpreted as the oldest fossil evidence for arcellinids, a modern group of testate (shell-forming) amoebozoans (Lahr et al. 2019; Porter and Riedman, 2019). The fossils left behind by these ancient amoebae are typically flask-shaped or hemispherical tests, ranging in length from ~40–300 μm, and are most often found preserved as casts and molds in a diverse array of preservation modes (Binda and Bokhari, 1980; Knoll and Calder, 1983; Kraskov, 1985; Green et al. 1988; Martí Mus and Moczydłowska, 2000; Porter and Knoll, 2000; Sergeev and Schopf, 2010; Straus et al. 2014; Cohen et al. 2017; Morais et al. 2017; Riedman et al. 2018; Martí Mus et al. 2020; and possibly Xiao et al. 2014). Because preservation is so diverse, most workers hypothesize that VSM test material was originally organic but secondarily mineralized (e.g., Porter and Knoll, 2000), consistent with ancestral state reconstructions of arcellinid test composition (Lahr et al. 2019; Porter and Riedman, 2019). VSMs are occasionally reported in shales, cherts, and carbonates preserved with carbonaceous test walls (Bloeser et al. 1977; Bloeser, 1985; Knoll and Calder, 1983; Vidal, 1979; Knoll et al. 1991; Horodyski, 1993; Morais et al. 2017; Riedman et al. 2018), though many reports are not confirmed.

Bloeser (1985) reported organic VSMs from shales of the Chuar Group, Grand Canyon, Arizona, based on electron probe microanalysis evidence for carbonaceous test walls. Porter and Knoll (2000) were unable to examine the specimens described by Bloeser (1985), but they did examine VSMs in shales from the same part of the stratigraphic column, and interpreted them to be siliceous casts coated internally and externally with organic

residue (Figure 1B; also see Porter and Knoll, 2000: figure 7C). As a result, they questioned whether the specimens described by Bloeser (1985) (Figure 1C) were actually original organic material. Recently, we were able to obtain the original specimens and samples that Bloeser studied. The goal of this research was to reexamine this material and determine if these VSMs are in fact preserved with original organic tests.

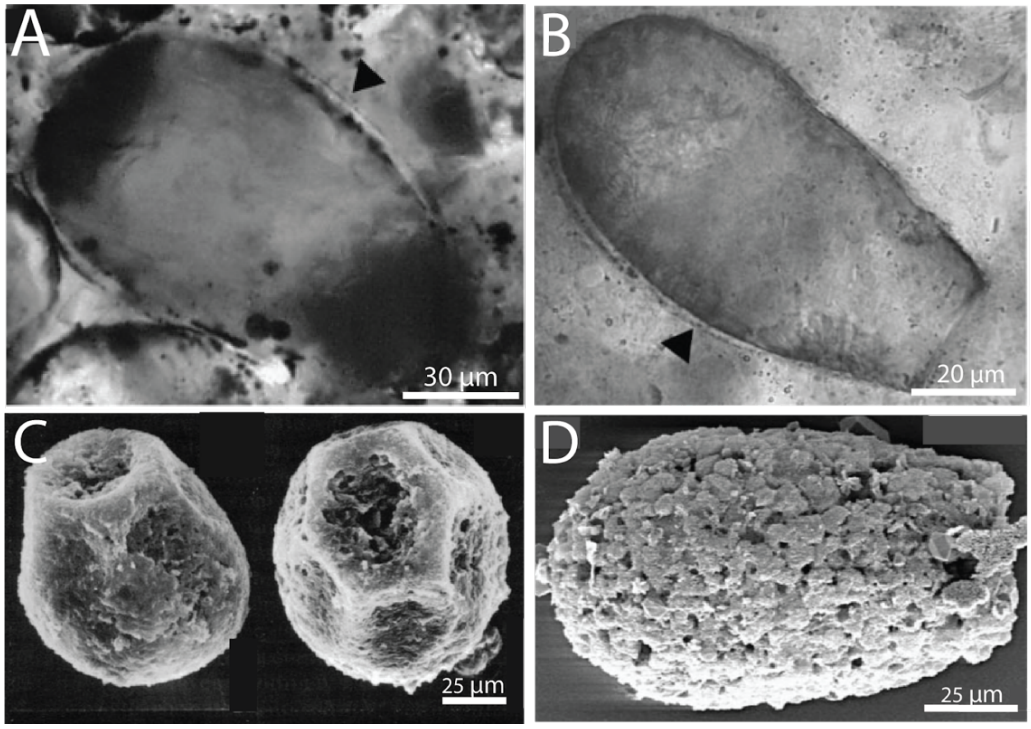

Figure 1: VSMs of the Chuar Group are reported as mineralized casts and molds and organically-preserved. *A*, *B*, VSMs occur in dolomite nodules in the upper Walcott Member reported as pyrite, iron-oxide, and organic coated casts and molds; *C,* organically-preserved tests in the lower Walcott Member; *D,* siliceous casts (interpreted as *possible* agglutinated tests) in shales in the upper Awatubi Member. Here, we test the hypothesis that the VSMs from shales of the lower Walcott Member contain original organic material. *A*, *B*, and *D* are from Porter and Knoll (2000) and *C* is from Bloeser (1985).

II. Geologic Background

The Chuar Group is a ~1600-m-thick succession of siltstone and mudstone interbedded with sandstone and dolomite (Ford and Breed 1973; Dehler et al. 2001) deposited in an extensional cratonic basin that formed in response to the rifting of Rodinia (Timmons et al., 2001; 2005). Exceptionally well-preserved Chuar Group strata are exposed along the western bank of the Colorado River in a 150-km^2 area of the eastern Grand Canyon, Arizona (Figure 2). The unit is disconformably overlain by the Cambrian-aged Sixtymile Formation (Ford and Breed 1973; Karlstrom et al. 2018). The Chuar basin is believed to have formed a tropical, epeiric sea in conjunction with the Pahrump Group basin, California, and the Uinta Mountain Group basin, Utah, and is correlated globally with the Mount Harper and Coates Lake groups, Canada and Akademikerbreen and lower Polarisbreen groups, Svalbard (Strauss et al. 2014; Dehler et al. 2017; Rooney et al. 2018).

The Chuar Group is divided in ascending order into the Nankoweap, Galeros, and Kwagunt formations, (Figure 3; Ford and Breed 1973; Dehler et al. 2017), the last of which contains VSM-bearing units. The Nankoweap Formation, a series of shallow marine siliciclastic deposits, is constrained to be <782 Ma from a U-Pb age of detrital zircons from basal beds (Dehler et al. 2017). The Galeros Formation comprises, in ascending order, the Tanner, Jupiter, Carbon Canyon, (757 ± 6.8 Ma, Rooney et al. 2018) and Duppa members, and includes a series of mudrocks interbedded with sandstone and dolomite. Sedimentological features show intermittent desiccation and symmetric ripples, and these, coupled with Os-isotope data suggest that these strata were deposited in a nonmarine to restricted basin setting, although it is likely there was at least some marine connection given

high pyrite content and the presence of marine fossils (Dehler et al. 2001; Porter and Riedman, 2016; Rooney et al. 2018). The Kwagunt Formation comprises, in ascending order, the Carbon Butte, Awatubi, and Walcott members, and records a transition to a period of marine transgression. The Awatubi Member consists of a basal stromatolite bed overlain by mudrocks. The overlying Walcott Member is a sequence of black mudrocks interbedded with dolomites that contain early diagenetic chert nodules and occasional thin pisolitic cherts (Dehler et al. 2001). The uppermost Walcott shales preserve dolomite nodules up to one meter in diameter (Porter and Knoll, 2000). The top of the Walcott Member is dated at 729.0 ± 0.9 Ma from U-Pb chemical abrasion–isotope dilution–thermal ionization mass spectrometry (CA-ID-TIMS) age from zircons within tuff (Rooney et al. 2018). Shales from the upper Walcott Member suggest euxinic conditions were prevalent (Johnston et al. 2010).

The Chuar Group contains diverse fossil assemblages in addition to VSMs, including ornamented organic-walled microfossils, *Chuaria*, phosphatic scale microfossils, stromatolites and biomarkers (Walcott, 1899; Ford and Breed 1973; Horodyski and Bloeser, 1983; Bloeser, 1985; Summons, 1988; Horodyski, 1993; Porter and Knoll, 2000; Porter and Riedman, 2016; Brocks et al. 2016; Zumberge et al. 2019; Riedman et al. 2021). VSMs first appear in the Kwagunt Formation in upper Awatubi Member shales and are reported as carbonaceous tests and siliceous, possibly agglutinated, casts (Horodyski, 1993; Porter and Knoll, 2000). Carbonaceous VSMs (Bloeser et al. 1977; Bloeser, 1985) as well as organic-coated siliceous casts (Porter and Knoll, 2000) are reported in shales of the lower Walcott Member. Finally, VSMs are found in great numbers (up to 4000/mm^3) as siliceous and calcareous casts and molds, sometimes coated with pyrite and/or iron oxide, in dolomite

nodules within uppermost Walcott shales (Figure 1A; Porter and Knoll 2000; Porter et al. 2003).

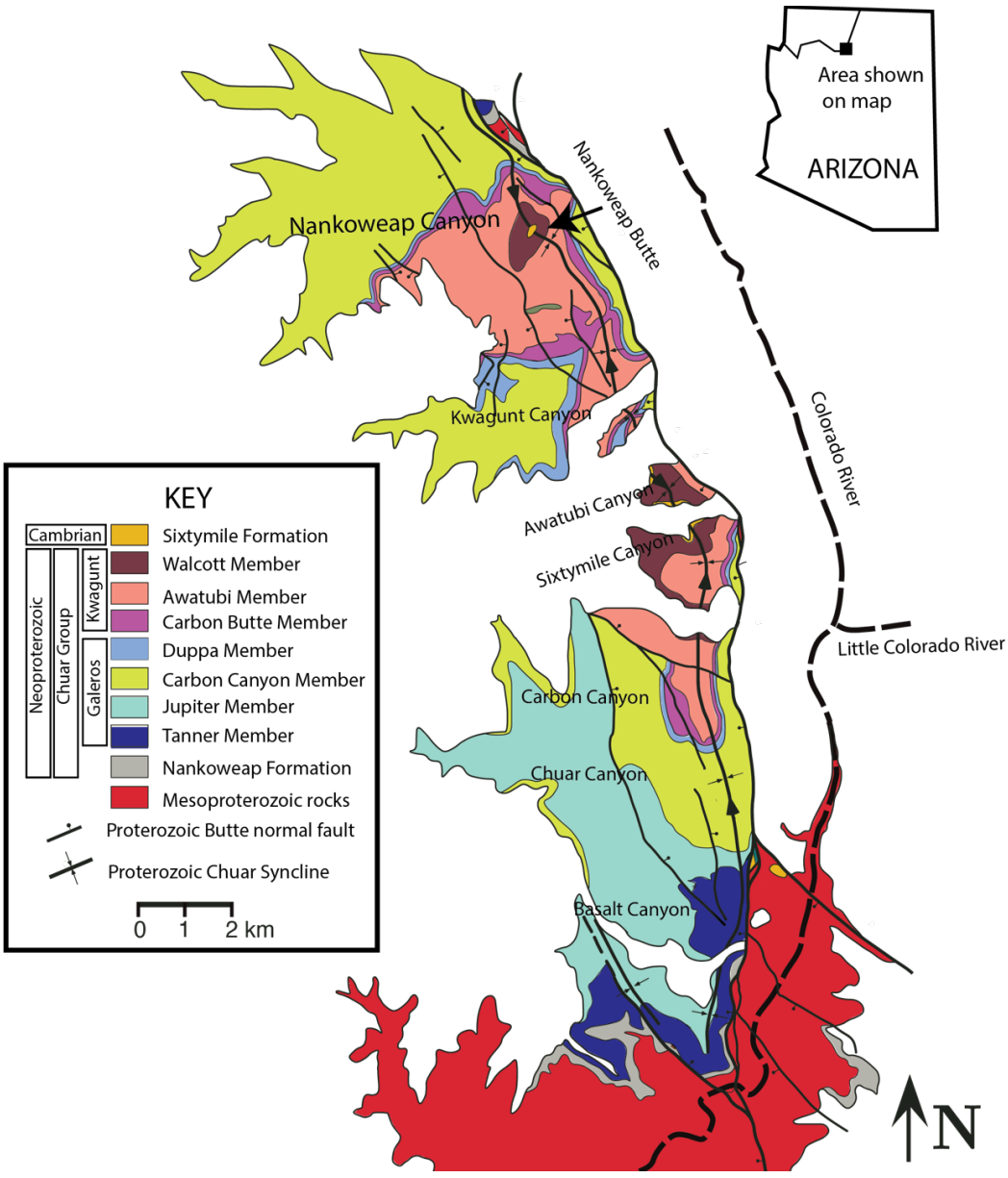

Figure 2: Geologic Map of the Chuar Group, northeastern Grand Canyon (modified from Timmons et al., 2001). VSMs are found in the Walcott Member (brown) and the Awatubi Member (peach). Shale samples for this study were taken from three localities on and around Nankoweap Butte, at 36°15'50" N and 111°53'22" W.

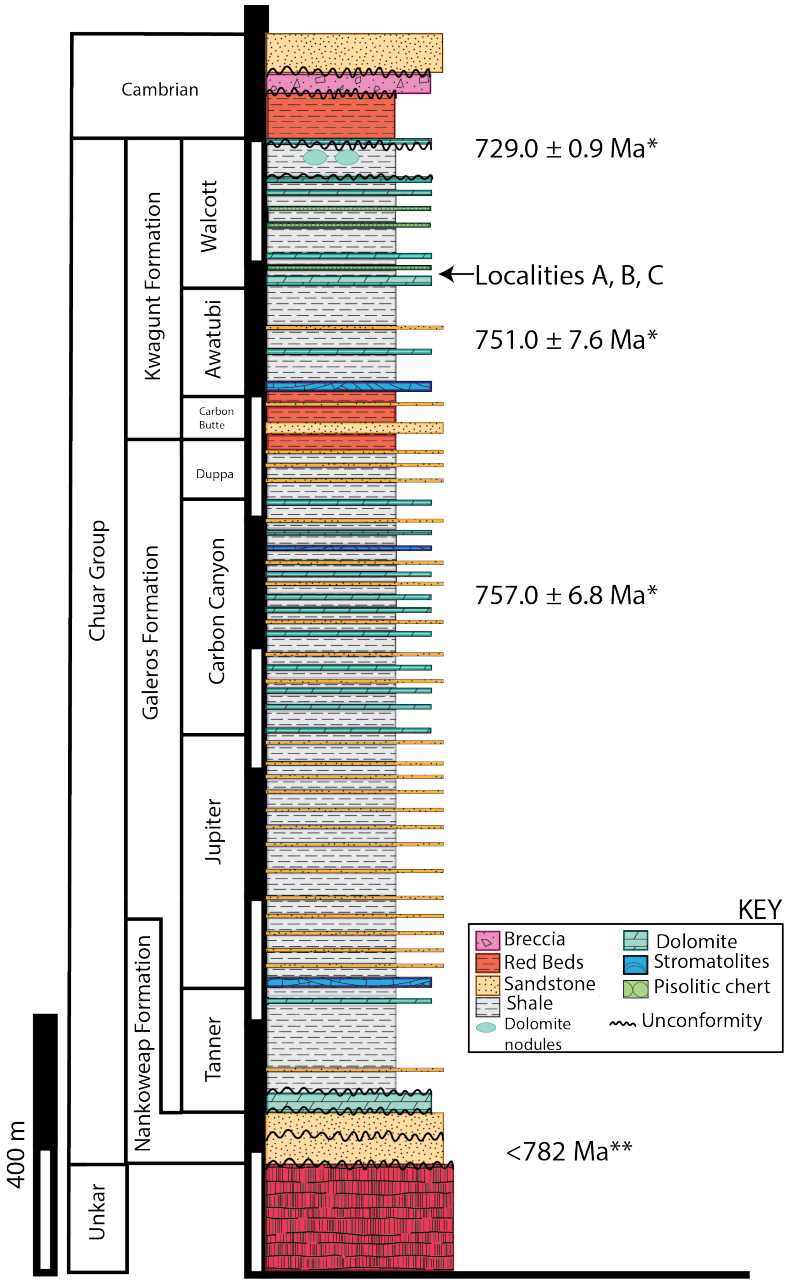

Figure 3. Stratigraphic section of the Chuar Group, Grand Canyon, Arizona. Redrawn from Dehler et al., 2017. The uppermost Walcott Member's age is constrained by a U-Pb zircon age from a tuff at 729.0 ± 0.9 Ma, with Re-Os ages on marcasite nodules of the Awatubi Member and organic-rich carbonates of the Carbon Canyon Member yielding ages of 751.0 ± 7.6 Ma and 757.0 ± 6.8 Ma, respectively (Rooney et al., 2018). The base of the Nankoweap Formation is <782 Ma based on U-Pb dating from detrital zircons (Dehler et al., 2017).

III. Materials and Methods

We identified VSMs using a Zeiss Axioskop 40 transmitted light microscope in polished thin sections cut perpendicular to bedding from two shale samples, Chuar Shale 2 and Chuar Shale 3 as denoted by B. Bloeser, from the lower Walcott Member. Shale samples were collected in the 1970s from three localities (A, B, C) at 36°15'50" N and 111°53'22" W: Locality A occurs ~3 m below the lowermost pisolite and above the basal dolomite bed; Locality B and C both occur on the northeast flank of Nankoweap Butte 1 m below a bed of black chert, about 450 m apart from one another (see Figure 3; Bloeser, 1985). We do not have records of which shale sample came from which locality, so it is unclear which of the localities (A, B, and C) Chuar Shale 2 and 3 belong to. Thin sections and shale samples are in the collections of S. Porter at UCSB. Thin sections are labeled CS2 and CS3, denoting Chuar Shale 2 or Chuar Shale 3, with additional numbering (.1, .2, .3) and lettering (A, B) for the purpose of organization, and thin sections are named along with England Finder coordinates in parentheses in figure captions. When possible, we identified VSMs to the genus and species level, and these identifications are specified in the figure captions.

We sputter-coated the thin sections with a ~3–5 nm-thick layer of a gold-palladium alloy (80:20) and used a FEI Quanta 400F field emission source scanning electron microscope (SEM) equipped with an INCAx-act silicon drift detector x-ray energy spectrometer at the Department of Earth Science, University of California, Santa Barbara to image VSMs. We operated the SEM at a working distance of ~10 mm with accelerating voltages between 10–15 kV and beam currents of ~.1–1 nA. We acquired secondary electron and/or backscattered electron signals to image VSM morphology and detect qualitative changes in sample mean atomic number (a proxy for chemical compositional variability).

We acquired individual 'spot/point' x-ray spectra from sample volumes of ~1–2 μm^3 that accumulated for ~30 seconds in order to assess local chemical composition. We developed x-ray intensity maps by scanning the electron beam across microfossils and adjacent matrix areas in order to assess variation in chemical composition.

We assessed elemental spatial variation with a Cameca SX100 equipped with 5 WDS spectrometers at the Department of Earth Science, University of California, Santa Barbara to. We tuned WDS spectrometers to the wavelength corresponding to the K-alpha characteristic x-ray emission for the elements Si, C, S, P and Fe. Maps of raw x-ray intensity were created by collecting 200 msecs of data on a grid pattern with 0.5 x 0.5μm^2 spacing (each map has a different number of pixels x-y). We used 20 nA of beam current, with 15 kV accelerating voltage, and a fully-focused electron beam. We processed the WDS elemental maps using the software ImageJ2. Brightness range is different for each of the five elements but is the same between samples, which allowed for comparison of relative abundance between samples from CS2 and CS3.

We measured the molecular structure of carbonaceous material within the microfossils and shale matrix of Walcott Member samples with a Horiba T64000 Raman system (Horiba, Inc., Edison, NJ) equipped with an Olympus BX41 microscope with 50x long working distance objective (numerical aperture = 0.50) and 457.9 nm excitation from a Coherent FreD 90C Ar+ laser with spot size of ~1 μm at the Department of Geology, University of Cincinnati. We used a neutral density filter to decrease the laser power to 1 mW. We collected and processed the data using the software LabSpec (v.5; Horiba, Inc., Edison, NJ).

IV. Results

A. Light Microscopy

VSMs of samples CS2 and CS3 vary in length from 44–132 µm (µ=78 µm; σ=20 µm; N=66), and in width from 34–104 µm (mean=56 µm; s.d.=16 µm; N=66). Test wall thickness varies from 1.2–5.6 µm (mean =2.4 µm; s.d.=0.8 µm; N=66) and is correlated to test length (Figure 4). When considering only carbonaceous VSMs (see mineralogy results below), test wall thickness varies from 1.2–3.3 µm (mean=2.0 µm; s.d.=0.6 µm; N=29). We identified *Cycliocyrillium torquata, Cycliocyrillium* sp.*, Bonniea dachruchares, Bonniea* sp.*,* and possibly *Trigonocyrillium horodyskii,* but it is impossible to distinguish *Cycliocyrillium* sp. from *Trigonocyrillium horodyskii* in transverse section given that they differ only in apertural shape.

In sample CS2, test walls appear translucent in transmitted light (Figure 5). All VSMs have a dark-colored material inside their tests; this material exhibits greater opacity in some VSMs than in others (compare Figure 5D vs. 5I). It appears to be connected to test walls in a web-like fashion (e.g., Figure 5I). There is a lighter-colored material dispersed throughout the tests, within the dark material.

In sample CS3, tests walls appear either translucent, usually with some mottling (Figure 6B, C) or opaque in transmitted and reflected light (Figure 6D, I). Like sample CS2, all VSMs have a dark-colored material inside their tests, but this material appears much more opaque and more cohesive than in sample CS2. In many VSMs, the material seems to retain the shape of the test and shows cracking patterns suggestive of desiccation (Figure 6B, F, H); these cracks are often filled in by a material that appears bright in transmitted light.

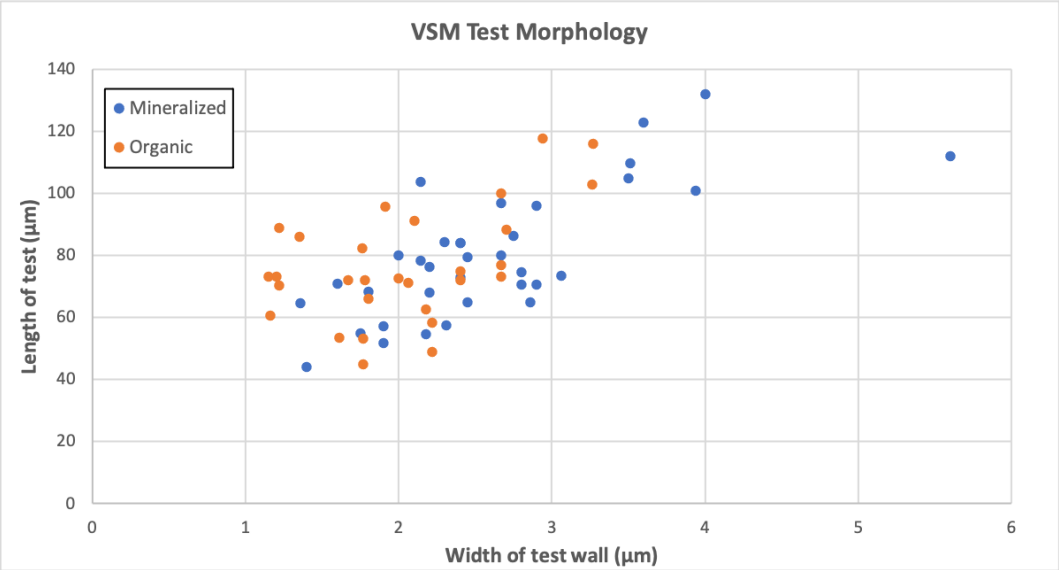

Figure 4. Correlation of length of VSM tests versus width of test walls (n=66). Organic VSMs are shown in orange and mineralized VSMs are shown in blue. The outlier with a thick test wall (see Figure 9M) likely has a thick, mineralized coating.

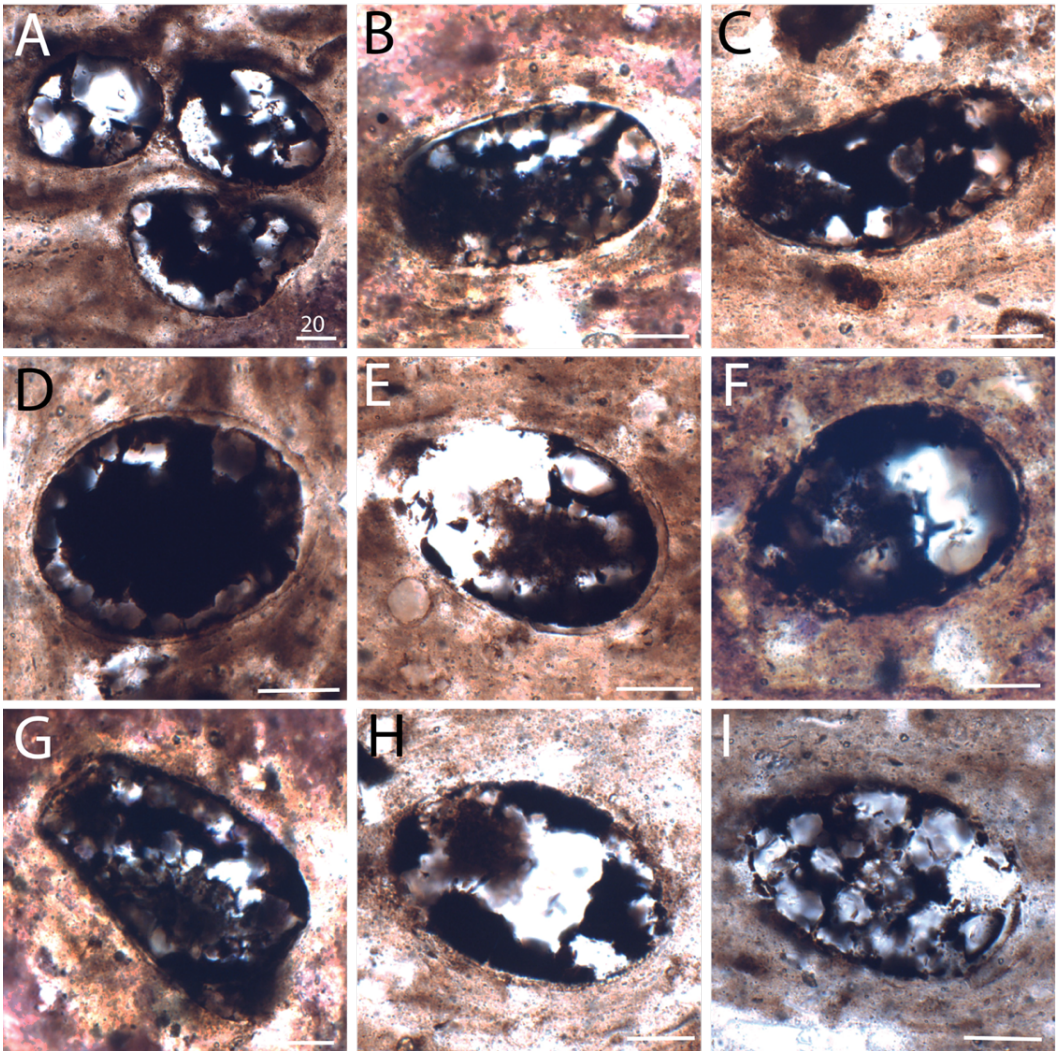

Figure 5. VSMs preserved with original organic tests from sample CS2 in transmitted light. All VSMs are filled with an opaque material, possibly bitumen, that is web-like in pattern. Organic test walls are translucent and sometimes mottled. *A*, (CS2.1A; V-41/1) *B*, (CS2.1A; K-51/4) *C, Bonniea dachruchares,* (CS2.1A; Q-66/2) *D,* (CS2.1A; O-52/4) *E*, (CS2.1A; X-59/3) *F*, (CS2.1A; G-49/3) *G,* (CS2.1A; K-51/3) *H,* (CS2.1A; Y-60) *I*, (CS2.1A; S-38/2). Scale bar = 20 µm.

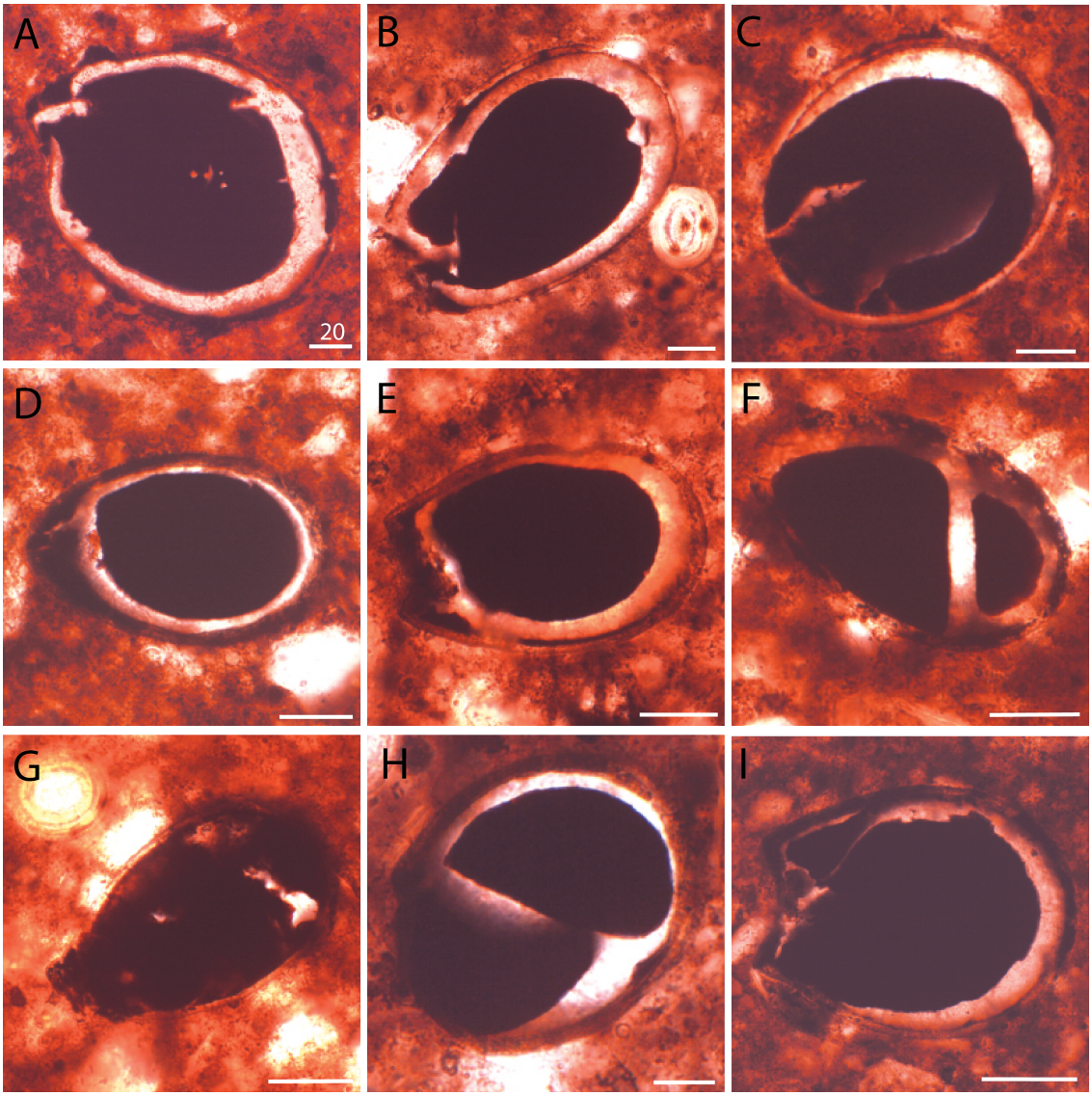

Figure 6. VSMs from sample CS3 in transmitted light. All VSMs are filled with an opaque material, possibly bitumen, that appears to have filled tests and subsequently shrunk and cracked, while retaining the overall shape of the test. VSMs from sample CS3 are preserved with original organic tests and as partial – complete casts made of pyrite, vivianite(?) and jarosite. Test walls are either opaque or appear translucent, sometimes displaying a mottled pattern. *A,* organic preservation of *Cycliocyrillium torquata;* (CS3.1; K-51/1). *B,* organic VSM; (CS3.1; Q-54/4). *C*, organic VSM; (CS3.1; S-56/2). *D*, complete cast; (CS3.1; R-41/1). *E,* partial cast; (CS3.1; V-53/3). *F*, complete cast; (CS3.1; T-55). *G*, *Cycliocyrillium torquata,* partial cast; (CS3.1; U-56/1). *H,* complete cast; (CS3.1; Q-42/3). *I,* complete cast; (CS3.1; L-45/4). Scale bar = 20µm.

B. Scanning Electron Microscopy and Electron Probe Micro-Analysis

Energy dispersive x-ray spectroscopy (EDS) spot analyses showed that test walls of VSMs from sample CS2 are mostly carbon with some silicon, aluminum, sulfur, and oxygen, and that the opaque internal material inside the VSMs is mostly carbon, with minor amounts of sulfur, aluminum, silicon, and oxygen. Given that, in life, cells are primarily made of water (e.g., Bratbak and Dundas, 1984), the opaque internal carbonaceous material must be exogenous. We will refer to the internal carbonaceous material as exogenous carbonaceous material (ECM) from here on, in addition to referring to the wall carbonaceous material (WCM). The matrix is enriched in aluminum, silicon, and oxygen, and the light-colored material observed within tests in optical microscopy contains silicon and oxygen (Figure S1). This silicon- and oxygen-rich internal material, likely quartz due to its chemistry and morphology in BSE/SE, occurs within and peripheral to the ECM (Figure 7B).

EDS spot analyses of VSMs of sample CS3 revealed two types of test walls. Test walls are either mostly carbon with some silicon, iron, sulfur, phosphorus, and aluminum (Figure S2), or mostly iron, sulfur, and phosphorus, with some silicon, aluminum, and sometimes carbon (Figure S3). The matrix is enriched in silicon (Figures S2, S3), and a platy, finely-crystalline Al-rich material, possibly kaolinite or another Al-rich clay mineral phase, is found in high concentrations within test interiors, in between the test walls and the ECM (Figures S2, S3, 8A, 8E, 8H). There also appear to be mineralized coatings, as some test walls appear anomalously thick (>4 μm, Figure 9M). BSE/SE imaging within some

specimens revealed the ECM to be two distinct materials. The first material is observed as a large central mass that is sometimes found still attached to test walls. The second material is darker in BSE than the larger central masses, and appears to have flowed through cracks in test walls, and to have thinly coated the interior and/or exterior of test walls (Figure 9F, 9J).

We used the electron probe micro-analyzer to gain a better understanding of the spatial distribution of silicon, carbon, iron, sulfur, and phosphorus. Wavelength dispersive x-ray spectroscopy (WDS) elemental maps show that in sample CS2, test walls are made of carbon and contain no silicon, and wall exteriors are lightly coated with sulfur and phosphorus. The ECM contains carbon and sulfur. The matrix has low concentrations of iron (Figure 10). In sample CS3, test walls contain carbon, iron, sulfur, and phosphorus, and wall exteriors appear to be additionally coated with phosphorus. Test walls contain no silicon. The ECM is made of carbon and sulfur. The matrix contains phosphorus, silicon, and iron (Figures 11-12). Within the sample, there are zones of relative iron enrichment and deficiency (Figure 13E).

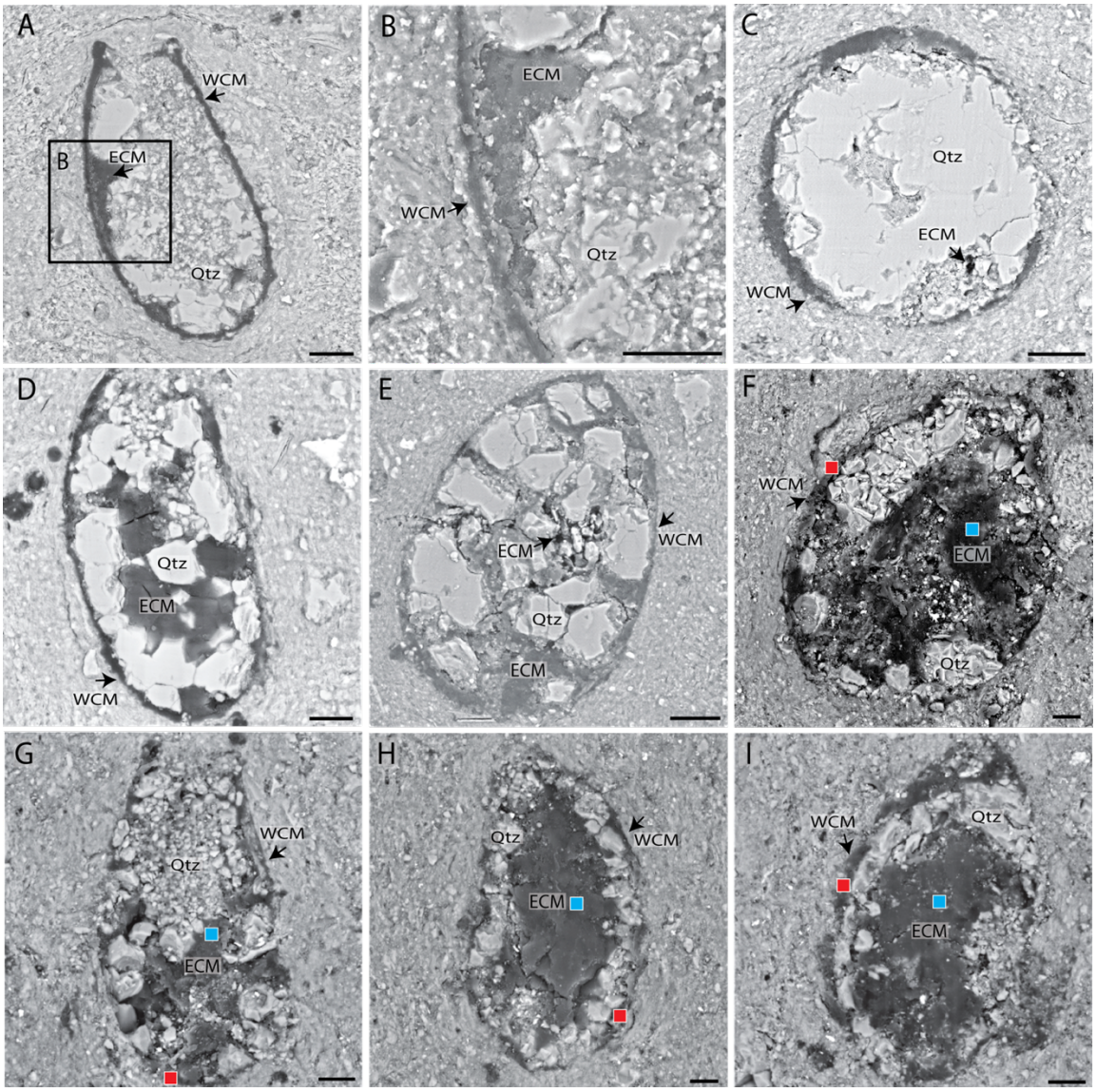

Figure 7. Backscattered electron images (BSE) images of carbonaceous VSMs from sample CS2. Note the presence of exogenous carbonaceous material (ECM) present in all VSMs in varying amounts, and the test wall carbonaceous material (WCM), which are separated often separated by microcrystalline quart (Qtz). Blue and red squares show the areas where we acquired Raman spectra (Figure 14) of the ECM and walls, respectively. *A, Bonniea dachruchares;* (CS2.1A; H-50/1). *B,* a magnification of the area shown in (*A*). *C*, (CS2.1A; U-39). *D, Bonniea sp.;* (CS2.1A; Q-66/2). *E,* (CS2.1A; S-38/2). *F, Cycliocyrillium torquata;* (CS2.1B; K-55/3). *G, Bonniea sp.;* (CS2.1B; R-60/3). *H, Bonniea sp.;* (CS2.1B; U-55/1). *I,* (CS2.1B; T-66/4). Scale bar = 10µm for all images.

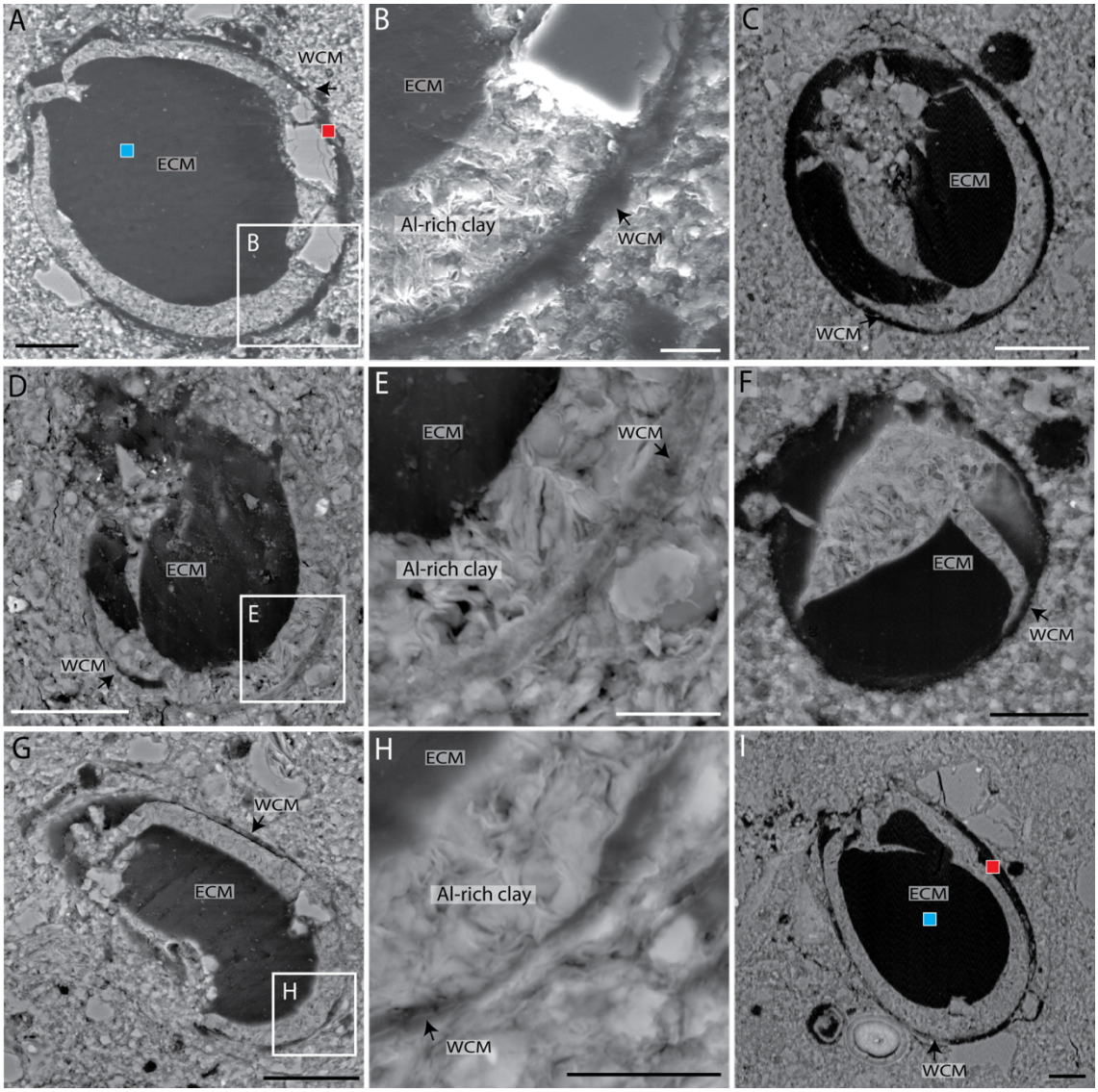

Figure 8. BSE images of carbonaceous VSMs from sample CS3. Note the extensive preservation of wall carbonaceous material (WCM) and how the exogenous carbonaceous material (ECM) holds the general shape of the VSM test, shows cracking patterns reminiscent of desiccation, and is surrounded by aluminum-rich clays. Blue and red squares show the areas where we acquired Raman spectra (Figure 14) of the ECM and walls, respectively. *A, Cycliocyrillium torquata*, (CS3.1; K-51/1). *B*, a magnification of the area pictured in (*A*), *C,* (CS3.1; S-56/2). *D,* (CS3.3; efc). *E,* a magnification of the area pictured in (*D*); (CS3.3; S-49/2). F, (CS3.2; Q-61/4). G, (CS3.3; L-45/4). *H,* a magnification of the area pictured in (*G*). *I,* (CS3.1; Q-54/4). Scale bar = 5 µm for *B, E, H*, and is 20 µm in all other images.

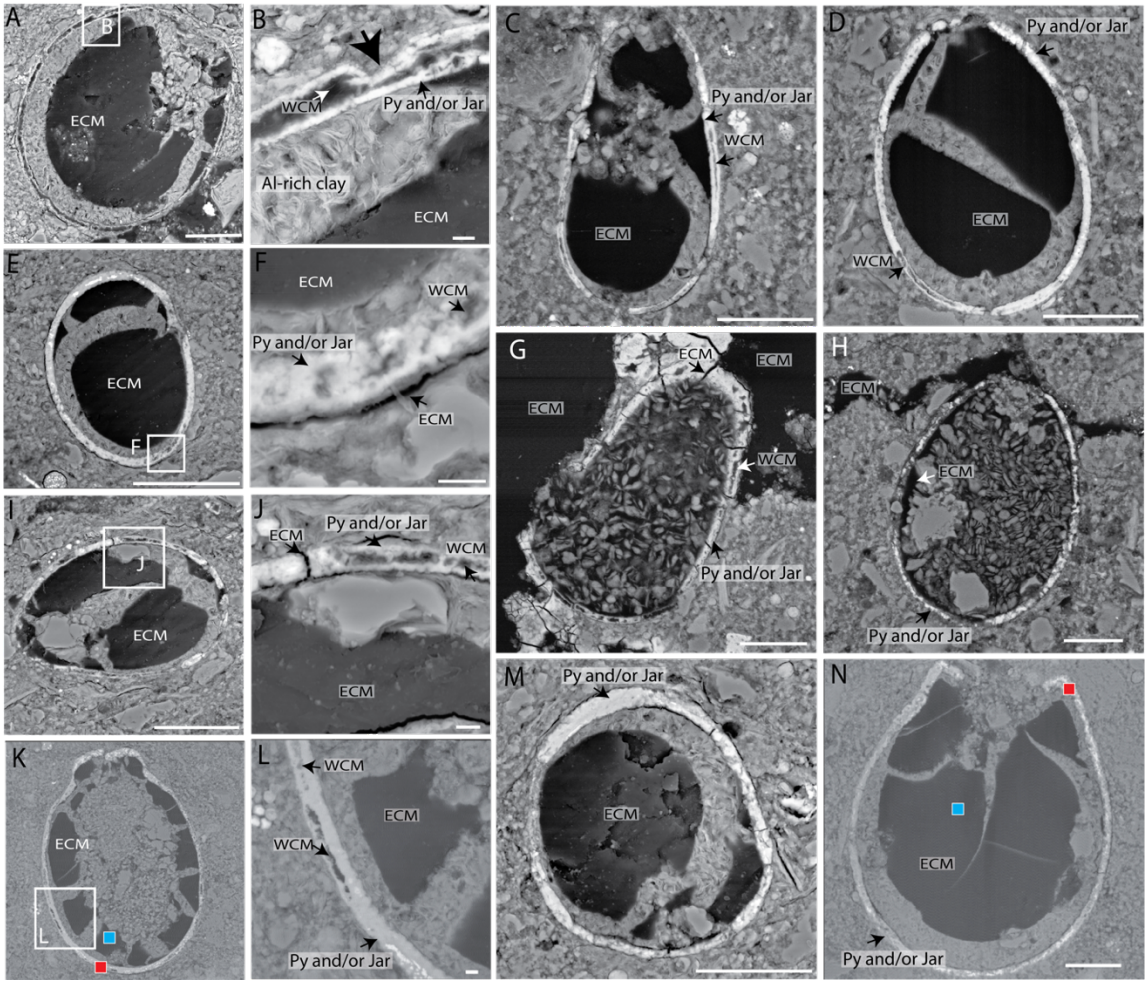

Figure 9: Backscattered electron images (BSE) of VSMs from CS3 showing partial and complete mineralization. Pyrite and vivianite(?) were the primary minerals that replaced the wall carbonaceous material (WCM), and pyrite was later variably oxidized to jarosite. Note the presence of exogenous carbonaceous material (ECM) inside of all VSMs, occurring directly adjacent to mineralized walls. The absence of any pyrite, vivianite(?) or jarosite associated with ECM likely indicates that the two carbonaceous materials are not coeval. Blue and red squares show the areas where we acquired Raman spectra (Figure 14) of the ECM and walls, respectively. *A,* a VSM with carbonaceous test wall partially mineralized; (CS3.3B; Q-55/2). *B,* a magnification of area specified in (*A*), showing a centripetal style of replacement. The large black arrow points to an indentation of the wall. This shows that replacement likely occurred early in diagenesis, prior to compaction. Note the presence of platy, Al-rich clay minerals. *C,* a partial cast of *Bonniea sp.*; (CS3.2; L-45). *D,E*, partial casts, (CS3.2; E-49/4 ; CS3.3; M-46/1). *F,* a magnification of the area specified in (*E*), which shows a thin coating of ECM on the exterior of the VSM. *G,* a partially mineralized VSM surrounded by a mass of ECM. This VSM appears to have been filled by ECM through cracks in the test walls; (CS3.2; V-51/4). *H,* a mineralized VSM in contact with a vein of ECM. The aperture appears to be plugged with detrital grains; (CS3.2; K-56/1). *K,* a partially mineralized *Cycliocyrillium torquata;* (CS3.1; Y-40/1). *L,* a magnification of the area shown in (*K*), showing centripetal replacement of the carbonaceous wall, although not as uniformly as in *A* and *B*. *M*, a cast that is likely coated, given its non-uniform thickness, (CS3.3; M-43/3). *N,* a complete cast, (CS3.1; L-45/4). Scale bar = 25 µm, except for (*B,F, J, L*), which = 2 µm.

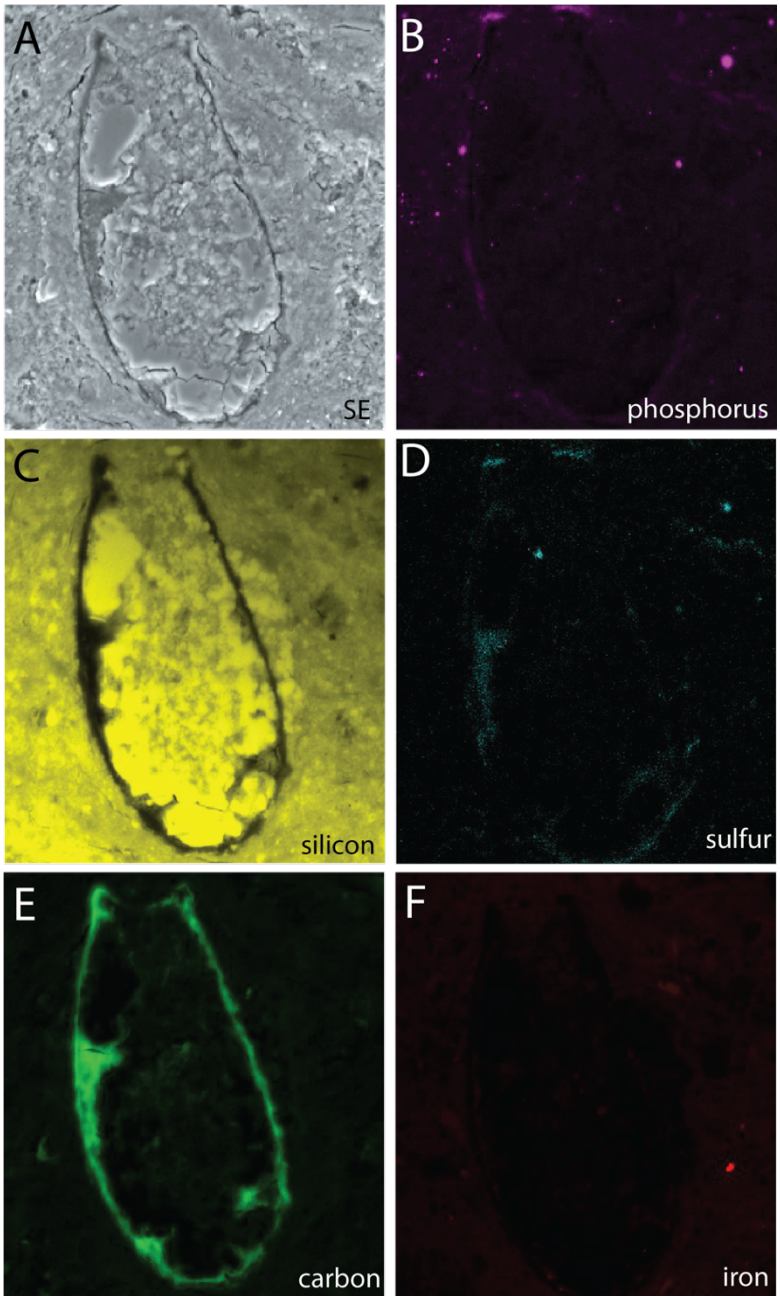

Figure 10: Elemental maps produced by electron probe micro-analysis of *Bonniea dachruchares* from sample CS2 showing carbonaceous wall preservation. Brightness corresponds to quantity of element; brighter colors indicate higher quantities, darkness indicate absence. Note the absence of silicon in the test walls. *A,* SE image. *B,* phosphorus. *C,* silicon. *D,* sulfur. *E,* carbon. *F,* iron. (CS2.1A; H-50/1)

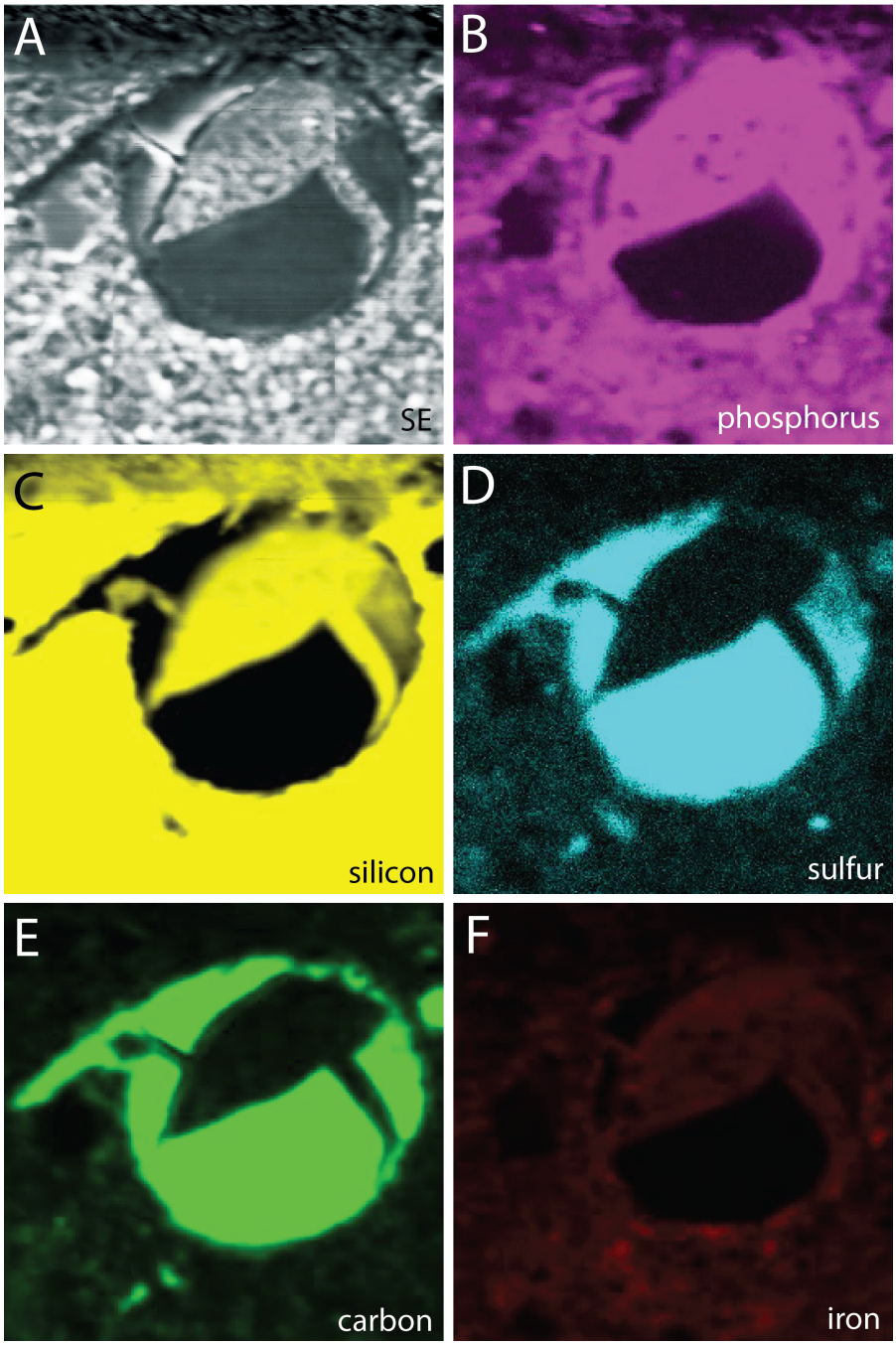

Figure 11: Elemental maps produced by electron probe micro-analysis of a VSM from sample CS2 showing organic preservation. *A,* SE image. *B,* phosphorus. *C,* silicon. *D,* sulfur. *E,* carbon. *F,* iron. (CS3.2; Q-61/4)

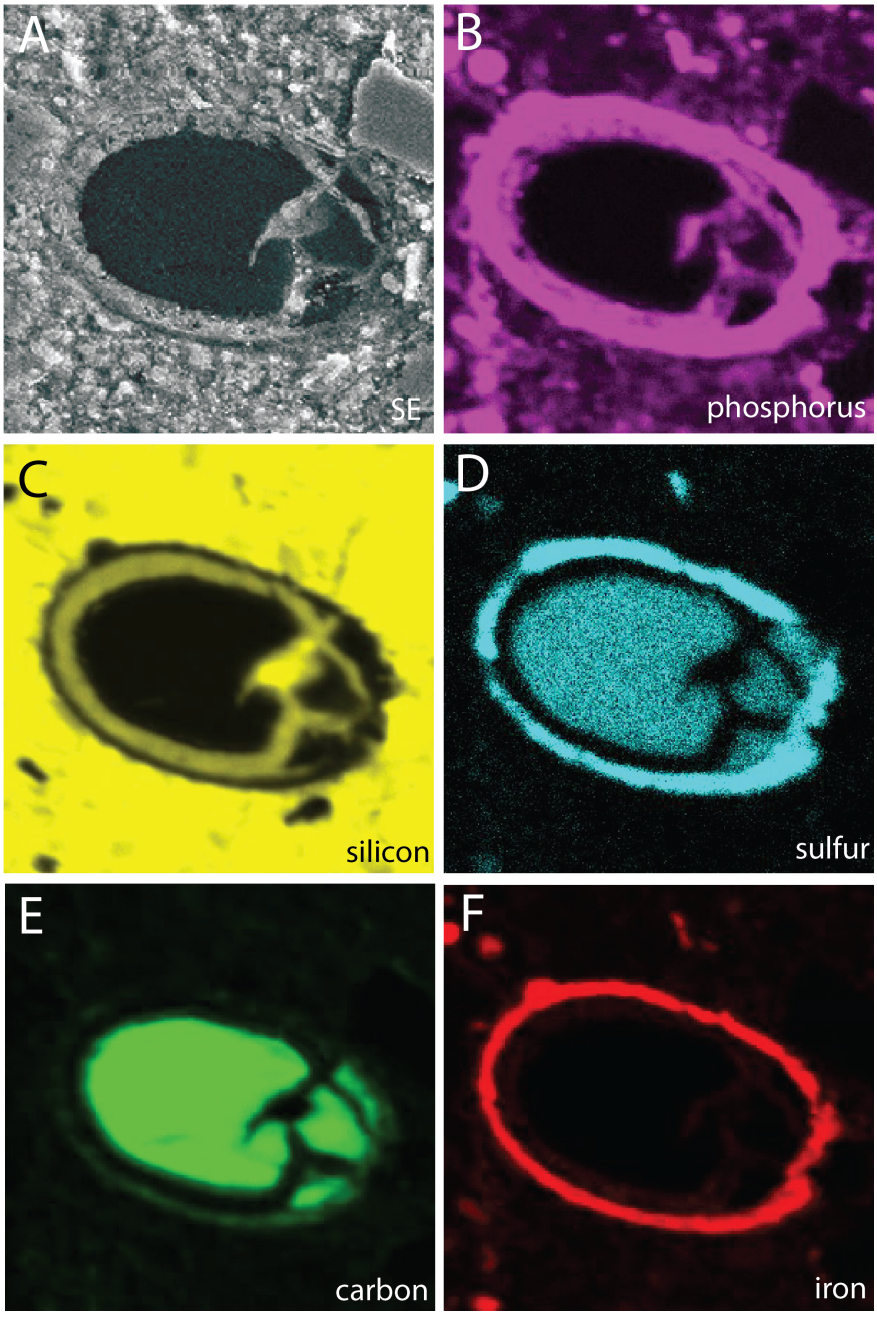

Figure 12: Elemental maps produced by electron probe micro-analysis of a VSM from sample CS2 showing secondarily mineralized wall composition. *A*, SE image. *B*, phosphorus. *C*, silicon. *D*, sulfur. *E*, carbon. *F*, iron. (CS3.2; Q-62/1)

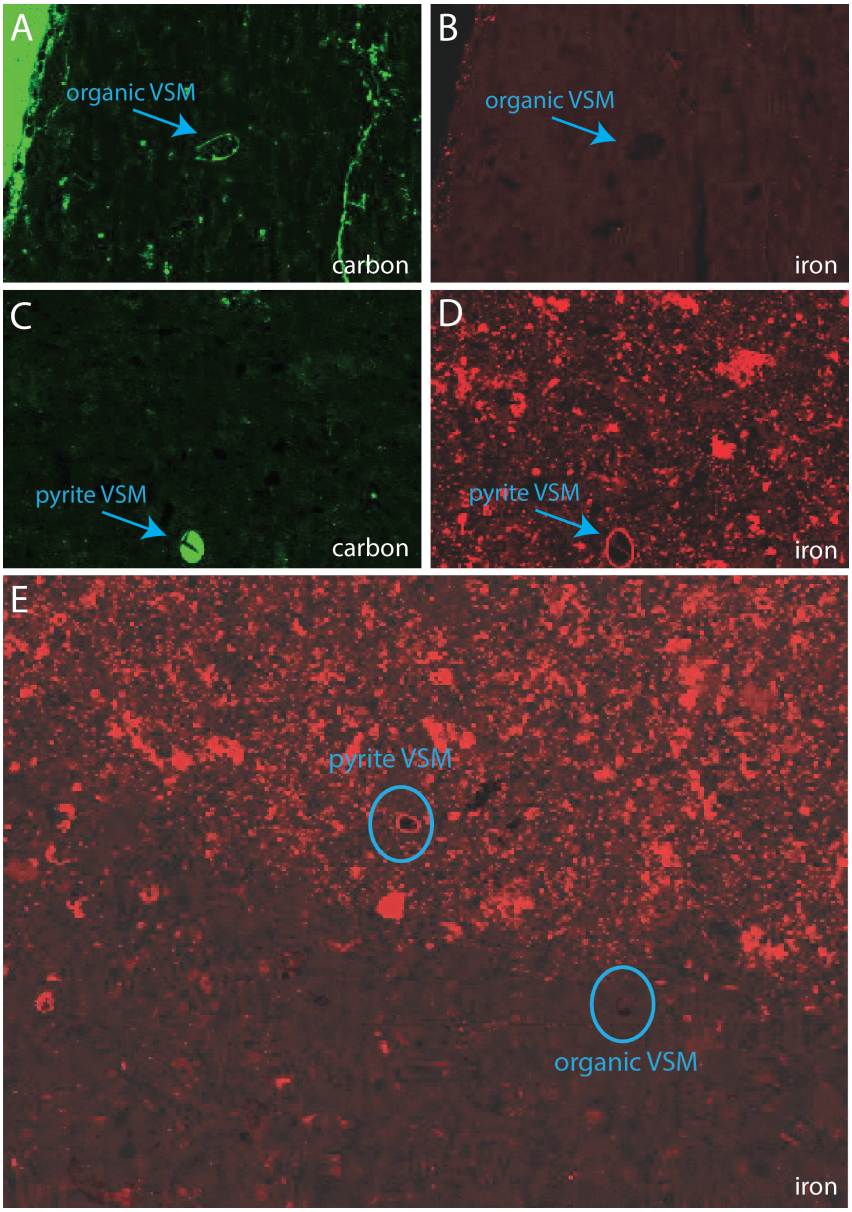

Figure 13. EPMA-WDS maps showing the spatial variation of carbon and iron concentrations within sample CS3 and between samples CS2 and CS3. Organic VSMs are associated with relatively iron-poor areas, and secondarily mineralized VSMs are associated with relatively iron-rich areas. *A,* carbon distribution in sample CS2; (CS2.1A). *B,* iron distribution within sample CS2, which is comparatively low; (CS2.1A). *C,* carbon distribution in sample CS3; (CS3.2). *D*, iron distribution within sample CS3, which is comparatively high: (CS3.2). *E,* a composite of iron and BSE image to show the location of VSMs and iron distribution. Note the presence of an organic VSM within an Fe-poor (darker red) zone; (CS3.2).

C. Raman Spectroscopy

Raman spectroscopy is a non-destructive analytical technique that can be used to examine the chemical composition of a material. Raman spectroscopy confirms that the silicon-oxygen mineral in VSMs of sample CS2 is quartz. The ECM and WCM of sample CS2 show prominent D (1350 cm^{-1}) and G (1580 cm^{-1}) bands that are similar in shape and intensity, suggesting both are composed of mature organic material, but the Raman spectra of the WCM are generally much noisier with higher background levels (Figure 14A, 14B). We observed that the matrix of sample CS2 is highly fluorescent when we looked at the sample with confocal microscopy; this fluorescence likely contributes to the noise in the spectra of the carbonaceous walls and the high background level (Figure S7).

Raman spectroscopy confirms that the iron-sulfur minerals found in the walls of VSMs of sample CS3 are pyrite and jarosite (Figure S4). The ECM and WCM of sample CS3 show prominent D and G bands that are similar in shape and intensity (Figure 14C, 14D), suggesting both are composed of mature organic material.

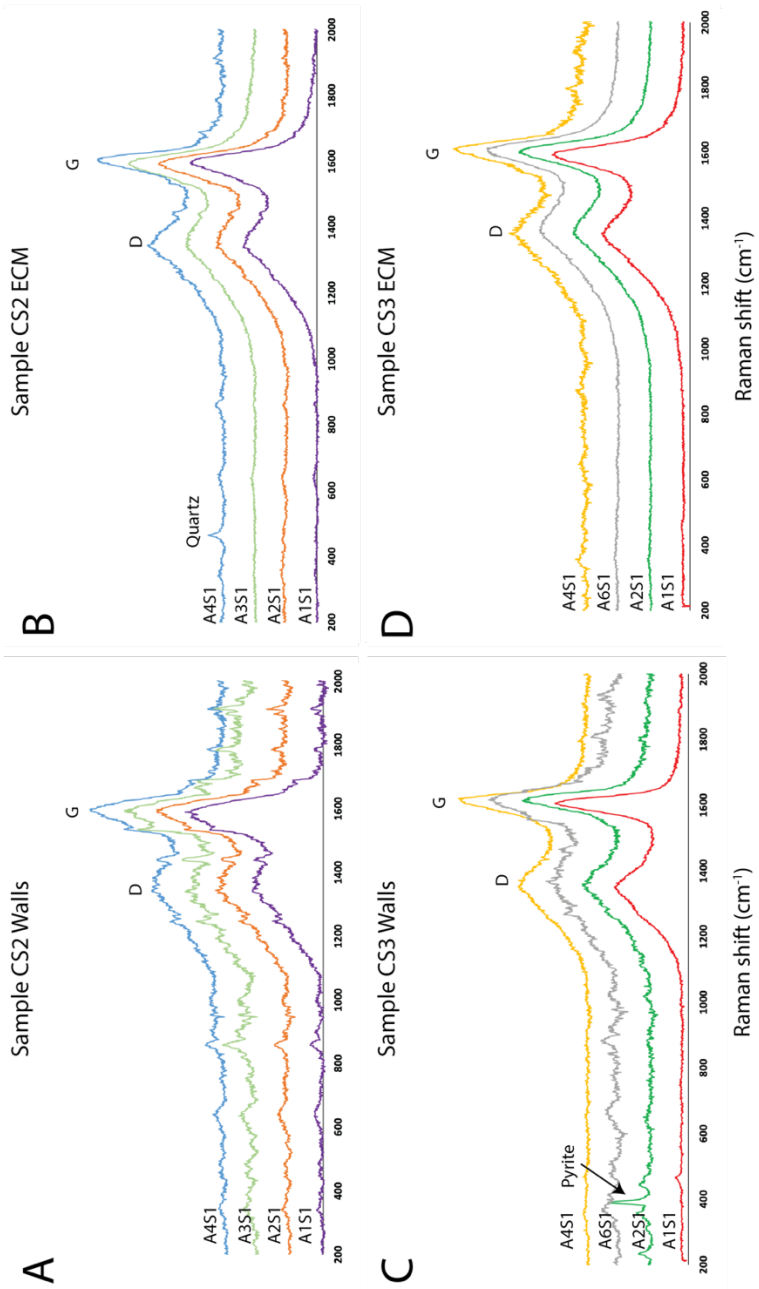

Figure 14. Baseline subtracted Raman spectra of test walls and exogenous carbonaceous material (ECM). The spectra of the WCM and the ECM materials are similar, which could imply similar chemical composition and/or thermal maturity. *A,* Raman spectra of walls in sample CS2, pictured in Figure 7, A1S1 is Fig. 7I, A2S1 is Fig. 7G, A3S1 is Fig. 7H, A4S1 is Fig.7F. *B,* Raman spectra of ECM in sample CS2, pictured in Figure 7 . *C,* Raman spectra of walls in sample CS3, pictured in Figures 8, 9, A1S1 is Fig. 8A, A2S1 is Fig. 9N, A4S1 is Fig. 9K, A6S1 is Fig. 8I. *D,* Raman spectra of ECM in sample CS2, pictured in Figures 8, 9.

V. Discussion

A. Carbonaceous material origin and timing of emplacement

We infer that the ECM found in test interiors is bitumen that matured within Walcott shales, because there are bituminous shales in both the Walcott and Awatubi members (e.g., Brocks et al., 2016), the matrices of both samples are organic-rich, and the carbonaceous material in the matrix revealed by Raman spectroscopy is similar to the ECM. The occurrence of ECM within test interiors and cracks in walls, partial attachment to test walls, and cracking patterns suggest that this material filled the entirety of the tests, and later shrunk and cracked (Figure 9C-E). This material may have filled the VSMs sometime in the Cretaceous or later, as burial history models predict that the Kwagunt Formation entered the oil window in the Cretaceous (Lillis, 2016). The Raman spectra of the WCM and ECM are similar, indicating comparable thermal maturity and/or chemical composition. This is consistent with bitumen forming in situ or nearby, maturing from organic material in or close to the Walcott shales.

How might bitumen have infiltrated VSM tests more than 600 million years after burial and lithification of the matrix? One possibility is that VSM tests were filled with fluid at the time of deposition, preventing detrital filling. By example, Buijs et al. (2004) found fluid within microborings in Pennsylvanian and Permian-aged brachiopods of Kansas, although the microborings are much larger than the VSM test interiors. It is possible that VSM tests could have been filled with fluid, possibly cell contents or porewater, at the time of cementation. Bitumen could have then permeated into test interiors and replaced the fluid. A second possible mode of preservation may have involved the infilled mineralization of the

test cavity during diagenesis, and it is possible that the quartz seen in test interiors in sample CS2 are partial or near complete internal molds.

B. Preservational modes of VSM test walls from the Walcott Member Shales

Spatial relationships among elements can tell us something about the mechanisms that allowed for preservation of fossil material. We interpret the mineral distribution observed in sample CS3 to represent replacement and coating of carbonaceous walls by pyrite and a phosphate mineral, possibly vivianite, which we will refer to as vivianite(?) (Figures 9, 12, 14, S4). Pyrite is known to form as a result of bacterial sulfate reduction (BSR), which oxidizes organic material while reducing sulfate to sulfide. Sulfides produced by BSR can react with Fe^{2+} and iron minerals to eventually precipitate pyrite in early diagenesis ($Fe^{2+} + S^0 + HS^- \rightarrow FeS_2 + H^+$; Berner 1970; Berg et al. 2020). Vivianite can form during sulfidic conditions ($3HS^- + 8H_2O + 6Fe^{III}PO_4 + H^+ \rightarrow 2Fe_3^{II}(PO_4)_2 \times 8H_2O + 2H_2PO_4^- + 3S^0$) and can form concurrently with pyrite if phosphate is available and sulfide concentrations are greater than 2.5mM (Berg et al. 2020). The jarosite ((K, Na, $H_3O)Fe^{3+}{}_3(SO_4)_2(OH)_6$) found in association with pyritized VSMs may have formed from the oxidation of pyrite (Zolotov & Shock, 2005). Thus, pyrite and vivianite(?) were likely the primary minerals in diagenetic alteration of test walls, and jarosite formed from pyrite as conditions changed to oxidative as the shales became exposed and weathered.

While the pyrite, vivianite(?) and jarosite are all secondary minerals that formed during sediment diagenesis, we propose that the carbonaceous material of the wall is primary. Consistent with this, most of the VSM walls are partially or entirely composed of carbon. However, the presence of bitumen inside the VSM tests complicates this matter, as it

raises the possibility that the carbonaceous walls may be the result of organic material that filled in a void created by the degradation of the original wall material. This phenomenon has recently been observed in microfossil assemblages in ca. 340 Ma cherts of the Red Dog Zn-Pb Deposit, Alaska, and 1.88 Ga cherts of the Gunflint Formation, Canada; although the microfossils within both of these assemblages appeared to all be preserved with original organic material, closer examination revealed that some may be siliceous molds that have been infiltrated with oil (Rasmussen & Muhling, 2019; Rasmussen et al. 2021).

However, we interpret the test walls observed here to be primary organic carbon that is unrelated to the ECM. First, there is a clear distinction of the two materials in transmitted light microscopy (Figures 5, 6). The test walls appear translucent, while the ECM is opaque. In addition, if the organic walls of the VSMs reflect secondary filling of mineralized casts by oil, we might expect to also see evidence of mineralized (most likely siliceous, given calcium was not found associated with the microfossils when analyzed with EDS) casts or molds infiltrated with bitumen. However, EPMA-WDS elemental mapping shows an absence of silicon in the walls of the organically-preserved VSMs (Figures 10, 11). Moreover, we observed extensive pyrite and vivianite(?) replacement of WCM in VSMs of sample CS3, but the ECM was never found to contain any evidence of pyrite or vivianite(?) formation, even in areas where ECM was still attached to mineralized test walls (Figures 9, 12). Therefore, the ECM was likely emplaced at a different time than when mineral replacement occurred. Based on this evidence, we suggest the carbonaceous test walls are distinct from the ECM and are made of mature organic material (e.g., kerogen) that reflects the original test wall.

C. Controls on organic preservation

Organic-walled microfossils, which make up the bulk of the Precambrian body fossil record, are ubiquitously preserved with original organic material (likely the remains of recalcitrant materials such as cysts and sheaths) in various lithologies. In contrast, VSM tests are rarely reported preserved with original organic material preserved. This may suggest that VSMs were made of more reactive material than organic-walled microfossils (Riedman et al. 2018). If so, special conditions must have been present in these shales that inhibited the decay of the VSMs.

Although clay minerals have been implicated in the preservation of organic material, there is no clear association observed here between clay minerals and organic preservation, such as the development of clay templating, clay mineral zonation, or aluminosilicate haloes around fossil material (e.g., Orr et al. 1998; Wacey et al. 2014; Anderson et al. 2018; Anderson et al. 2020). Though we found aluminum-rich clay minerals around the ECM of VSMs of sample CS3, these clay minerals fill in the cracks and spaces left by the shrunken bitumen, possibly via adsorption (Liu et al. 2014), suggesting that they formed after hydrocarbon infiltration. If this bitumen originated in the Cretaceous or later (Lillis, 2016), these clay minerals are likely not relevant to organic preservation. Moreover, all of the VSMs of sample CS2 are organically preserved, but we observed no clear association of organic tests with clay minerals, such as those described above.

Instead, we speculate that the organic preservation may be a result of sulfurization. During sulfurization, which may happen in sediments or in the water column, sulfur atoms are incorporated into organic compounds by reacting with certain functional groups that are common in lipids and carbohydrates. This transformation makes organic material less

available for degradation, and thus aids in preservation (Brassell et al. 1986; Sinninghe Damsté and De Leeuw, 1987; Sinninghe Damsté and De Leeuw, 1990; Werne et al. 2008; Raven et al. 2021). Sulfurization may have played an important role in the preservation of large quantities of organic matter during the ocean anoxic events of the Cretaceous (Raven et al. 2018; Raven et al. 2021) and has been shown to have influenced the preservation of organelles, biomarkers, and invertebrate soft tissue (Melendez et al. 2013; McNamara et al. 2016). The three conditions thought to be necessary for sulfurization to occur are sufficient levels of reduced sulfur, sufficient amounts of functionalized organic matter, and low levels of reactive iron (Werne et al. 2004). Consistent with this, we observed sulfur associated with organic test walls (Figure 10D, 11D), high TOC in both samples (sample CS2=1.54 ± .06 wt%, sample CS3=3.00 ± .06 wt%: Woltz et al. 2021), and low iron concentrations associated with organic VSMs (Figure 13). Thus, sulfurization may have been a factor in the preservation of organic VSMs, but more work, possibly by using x-ray absorption spectroscopy to identify the speciation of organic sulfur within the microfossil material, is needed to determine if there is in fact a robust association.

We observed a preservational gradient between complete organic preservation and complete mineralization (Figure 15) and suggest that variation in the ratio of iron to functionalized organic matter (i.e., organic matter that is reactive) could have promoted the preservation modes observed (Figure 16). Schiffbauer et al. (2014) observed a similar taphonomic gradient and proposed a model in which sedimentation rate variation can promote such a gradient. It is possible that the preservation seen in this study is a result of variation in sedimentation rate, although the difference in size between the specimens in Schiffbauer et al. (2014) and the specimens in this study must be considered. Because of the

small size of these fossils, the time scale of organic matter degradation and subsequent mineralization may potentially be much faster than at the sedimentation rate scale. Recent studies have shown that, facilitated by sulfate-reducing microbial activity, pyrite and vivianite can form in weeks to months under sulfidic conditions (Berg et al. 2020; Duverger et al. 2020). Thus, the VSMs could have been mineralized shortly after deposition in the sediments, or if euxinic conditions were present, even in the water column.

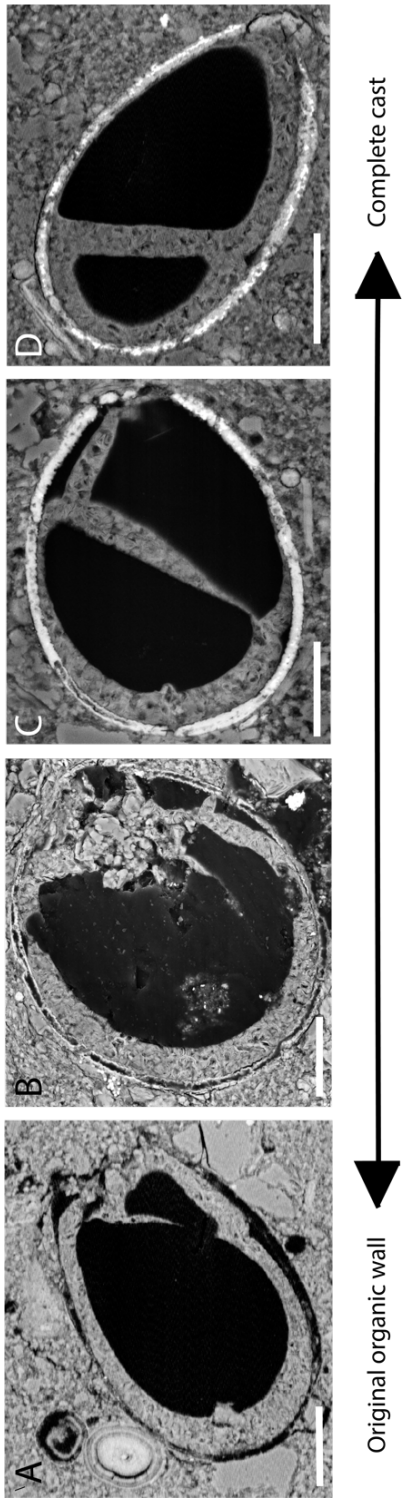

Figure 15. Organic–Mineralization preservational gradient. We observed a continuum in preservation modes of VSMs from sample CS3. (*A),* organic preservation; (CS3.1; Q-54/4). *(B)* partial organic preservation, partial mineralization; (CS3.3; Q-55/2). (*C)* near complete mineralization; (CS3.2; E-49/4). (*D),* complete mineralization; (CS3; T-55). Scale bar = 25 µm.

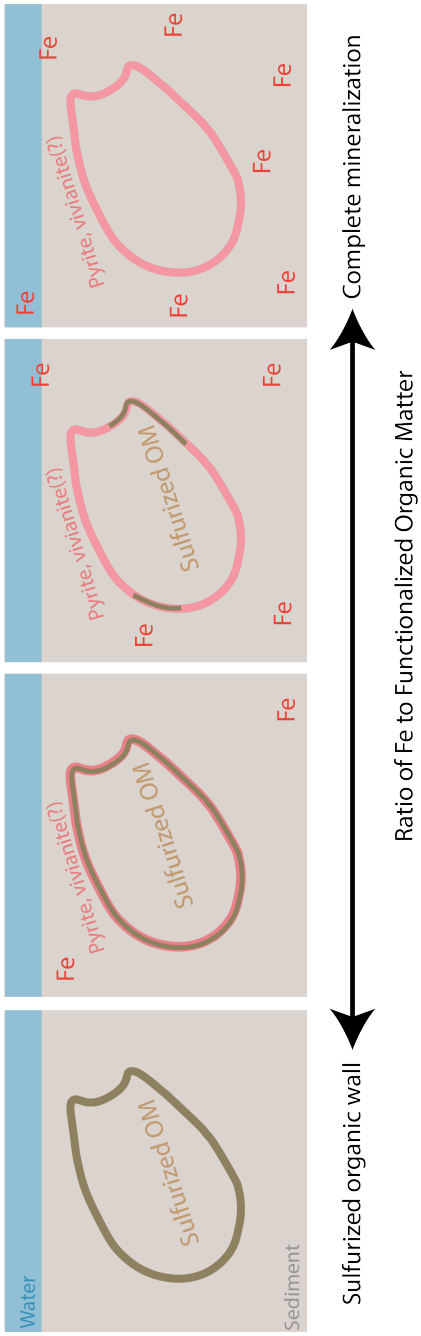

Figure 16. Proposed model of preservation, dependent on the ratio of iron to functionalized organic matter. Sulfurized organic material (OM) is shown in olive and pyrite and vivianite(?) replaced walls are shown in pink. The blue area represents seawater and the grey area represents sediments. When the ratio of iron to functionalized organic matter is low, sulfurization of organic test material is extensive and organic preservation is observed. When the ratio is high, complete mineralization is observed.

D. Comparison to other VSMs reported globally from Neoproterozoic units

While a handful of other VSM assemblages are thought to show organic preservation (Knoll and Calder, 1983; Vidal, 1979; Knoll et al. 1991; Morais et al. 2017; Riedman et al. 2018), the majority of reports are of siliceous or calcareous casts and molds, (sometimes with pyrite and/or iron oxide coatings), or as pyrite or iron oxide casts and internal molds (Binda and Bokhari, 1980; Knoll and Calder, 1983; Kraskov, 1985; Green et al., 1988; Porter and Knoll, 2000; Sergeev and Schopf, 2010; Cohen et al., 2017; Riedman et al., 2018, Martí Mus et al., 2020). Only a few of the studies cited, however, have included compositional and mineralogical data to support their taphonomic interpretations of organic preservation or secondary mineralization (Cohen et al. 2017; Morais et al. 2017; Martí Mus et al. 2020).

Our observations suggest that organic VSMs may be more widespread than currently recognized. The organic tests observed here are mostly colorless and appear translucent in transmitted light microscopy. Porter and Knoll (2000) interpreted translucent-walled VSMs from this same stratigraphic horizon to be organic-coated siliceous casts, but they performed no geochemical analyses. It is possible that the VSMs they observed are siliceous casts, but as we saw no evidence for siliceous casts in our samples, it is more likely they were observing organically-preserved VSMs.

E. Test composition and implications

Modern arcellinids build their tests from protein (Ogden, 1984). Given that VSMs are thought to be early arcellinids (Lahr et al. 2019; Porter and Riedman, 2019), it seems reasonable to assume that VSM test material was also proteinaceous in life. Proteins have

low preservation potential compared to other molecules like complex carbohydrates and lipids, nevertheless, workers have detected proteins preserved in Mesozoic and even Paleozoic fossil animals (Cody et al. 2011; Briggs and Summons, 2014; Lee et al. 2017; Myers et al. 2018). If the VSMs are proteinaceous (though likely heavily modified by diagenesis), it would extend the fossil record of proteins into the Neoproterozoic, and possibly offer insight into testate amoebozoan evolution. Future work should compare organically-preserved VSM composition with modern arcellinid test composition, possibly with photo-emission electron spectroscopy (PEEM) in tandem with X-ray absorption near-edge structure (XANES) spectroscopy, as was recently used in Myers et al. (2018) to compare the proteinaceous matrix material of Cretaceous mollusks with that of modern mollusks.

VI. Conclusion

VSMs from black shales of the lower Walcott Member of the Chuar Group, Grand Canyon, AZ are preserved as original organic tests and as partial and complete casts made of pyrite, jarosite, and an iron phosphorus mineral we suggest may be vivianite. Pyrite and vivianite(?) replaced, and sometimes coated, primary organic test material, with jarosite forming later via the oxidation of pyrite. All VSMs are filled with a carbon-rich material that is possibly bitumen, probably generated within the Chuar Group during the Cretaceous, that subsequently infiltrated previously fluid-filled tests. We suggest that sulfide abundance, organic-rich sediments, and low levels of iron, facilitated sulfurization of organic test material, promoting organic preservation, and partial organic preservation may be controlled by variation in sedimentation rate. Organic VSMs are rarely reported, but in fact may be more widespread and simply overlooked, given that organic walls appear similar to mineralized walls under transmitted light.

References

Anderson, R. P., Tosca, N. J., Gaines, R. R., Koch, N. M., and Briggs, D. E., (2018). A mineralogical signature for Burgess Shale–type fossilization. *Geology*, *46*, 4, 347-350. https://doi.org/10.1130/G39941.1

Anderson, R.P., Tosca, N.J., Cinque, G., Frogley, M.D., Lekkas, I., Akey, A., Hughes, G.M., Bergmann, K.D., Knoll, A.H. and Briggs, D.E., (2020). Aluminosilicate haloes preserve complex life approximately 800 million years ago. *Interface Focus*, *10*, 4, 20200011. https://doi.org/10.1098/rsfs.2020.0011

Berg, J.S., Duverger, A., Cordier, L., Laberty-Robert, C., Guyot, F. and Miot, J., (2020). Rapid pyritization in the presence of a sulfur/sulfate-reducing bacterial consortium. *Scientific Reports*, *10*, 1, 1-13. https://doi.org/10.1038/s41598-020-64990-6

Berner, R.A., (1970). Sedimentary pyrite formation. *American Journal of Science*, *268*, 1, 1-23. https://doi.org/10.2475/ajs.268.1.1

Binda, P., and Bokhari, M.M., (1980). Chitinozoan-like microfossils in a late Precambrian Dolostone from Saudi Arabia. *Geology*, *8*, 70–71. https://doi.org/10.1130/0091-7613(1980)8%3C70:CMIALP%3E2.0.CO;2

Bloeser, B., (1985). Melanocyrillium, a new genus of structurally complex late Proterozoic microfossils from the Kwagunt Formation (Chuar Group), Grand Canyon, Arizona. *Journal of Paleontology*, *59,* 741-765. http://www.jstor.org/stable/1304994

Bloeser, B., Schopf, J.W., Horodyski, R.J. and Breed, W.J., (1977). Chitinozoans from the late Precambrian Chuar group of the Grand Canyon, Arizona. *Science*, *195*, 4279, 676-679. https://doi.org/10.1126/science.195.4279.676

Brassell, S.C., Lewis, C.A., De Leeuw, J.W., De Lange, F. and Sinninghe Damsté, J.S., (1986). Isoprenoid thiophenes: novel products of sediment diagenesis? *Nature*, *320*, 6058, 160-162. https://doi.org/10.1038/320160a0

Bratbak, G. and Dundas, I., (1984). Bacterial dry matter content and biomass estimations. *Applied and Environmental Microbiology*, *48*, 755-757. https://aem.asm.org/content/48/4/755

Briggs, D.E. and Summons, R.E., (2014). Ancient biomolecules: their origins, fossilization, and role in revealing the history of life. *BioEssays*, *36*, 5, 482-490. https://doi.org/10.1002/bies.201400010

Brocks, J.J., Jarrett, A.J.M., Sirantoine, E., Kenig, F., Moczydłowska, M., Porter, S.M., and Hope, J., (2016). Early sponges and toxic protists: possible sources of

cryostane, an age diagnostic biomarker antedating Sturtian Snowball Earth. *Geobiology*, *14,* 2, 129-149. https://doi.org/10.1111/gbi.12165

Buijs, G.J., Goldstein, R.H., Hasiotis, S.T. and Roberts, J.A., (2004). Preservation of microborings as fluid inclusions. *The Canadian Mineralogist*, *42*, 5, 1563-1581. https://doi.org/10.2113/gscanmin.42.5.1563

Cody, G.D., Gupta, N.S., Briggs, D.E., Kilcoyne, A.L.D., Summons, R.E., Kenig, F., Plotnick, R.E. and Scott, A.C., (2011). Molecular signature of chitin-protein complex in Paleozoic arthropods. *Geology*, *39*, 3, 255-258. https://doi.org/10.1130/G31648.1

Cohen, P.A., Irvine, S.W., & Strauss, J.V., (2017). Vase-shaped microfossils from the Tonian Callison Lake Formation of Yukon, Canada: taxonomy, taphonomy and stratigraphic palaeobiology. *Palaeontology*, *60*, 5, 683-701. https://doi.org/10.1111/pala.12315

Dehler, C. M., Elrick, M., Karlstrom, K. E., Smith, G. A., Crossey, L. J., and Timmons, J. M., (2001). Neoproterozoic Chuar Group (~ 800–742 Ma), Grand Canyon: A record of cyclic marine deposition during global cooling and supercontinent rifting. *Sedimentary Geology*, *141*, 465-499. https://doi.org/10.1016/S0037-0738(01)00087-2

Dehler, C., Gehrels, G., Porter, S., Heizler, M., Karlstrom, K., Cox, G., Crossey, L. and Timmons, M., (2017). Synthesis of the 780–740 Ma Chuar, Uinta Mountain, and Pahrump (ChUMP) groups, western USA: implications for Laurentia-wide cratonic marine basins. *GSA Bulletin*, *129*, 607-624. https://doi.org/10.1130/B31532.1

Duverger, A., Berg, J.S., Busigny, V., Guyot, F., Bernard, S. and Miot, J., (2020). Mechanisms of pyrite formation promoted by sulfate-reducing bacteria in pure culture. *Frontiers in Earth Science*, *8*, 588310. https://doi.org/10.3389/feart.2020.588310

Ford, T. D., and Breed, W.J., (1973). Late Precambrian Chuar Group, Grand Canyon, Arizona. *GSA Bulletin, 84*, 1243– 1260. https://doi.org/10.1130/0016-7606(1973)84%3C1243:LPCGGC%3E2.0.CO;2

Green, J.W., Knoll, A.H., and Swett, K., (1988). Microfossils from oolites and pisolites of the upper Proterozoic Eleonore Bay Group, central East Greenland. *Journal of Paleontology 62*, 6, 835–852. https://www.jstor.org/stable/1305372

Horodyski, R.J., (1993). Paleontology of Proterozoic shales and mudstones: examples for the Belt Supergroup, Chuar Group and Pahrump Group, western USA. *Precambrian Resesarch,61,* 241–278. https://doi.org/10.1016/0301-9268(93)90116-J

Horodyski, R. J., and Bloeser, B. (1983). Possible eukaryotic algal filaments from the Late Proterozoic Chuar Group, Grand Canyon, Arizona. *Journal of Paleontology*, *57*, 321–326. https://www.jstor.org/stable/1304656

Karlstrom, K.E., Bowring, S.A., Dehler, C.M., Knoll, A.H., Porter, S.M., Marais, D.J.D., Weil, A.B., Sharp, Z.D., Geissman, J.W., Elrick, M.B. and Timmons, J.M., (2000). Chuar Group of the Grand Canyon: Record of breakup of Rodinia, associated change in the global carbon cycle, and ecosystem expansion by 740 Ma. *Geology*, *28,* 7, 619-622. https://doi.org/10.1130/0091-7613(2000)28%3C619:CGOTGC%3E2.0.CO;2

Knoll, A.H., and Calder, S., (1983). Microbiotas of the late Precambrian Ryssö Formation, Nordaustlandet, Svalbard. *Palaeontology*, *26*, 3, 467–496. http://pascal-francis.inist.fr/vibad/index.php?action=getRecordDetail&idt=PASCALGEODEBRGM8320486921

Knoll, A.H., Swett, K., and Mark, J., (1991). Paleobiology of a Neoproterozoic tidal flat/lagoonal complex: the Draken Conglomerate Formation, Spitsbergen. *Journal of Paleontology, 65*, 4, 531–570. https://www.jstor.org/stable/1305669

Kraskov, L. N., (1985). Находка проблематических организмов в отложениях Чаткарагайскоа свиты (Таласский хребет) (Finding of problematic organisms in sediments of Chatkaragai Suite (Talas Ridge)). Академии наук СССР, Труды (*USSR Academy of Sciences, Proceedings*), *632*, 149–152.

Lahr, D.J., Kosakyan, A., Lara, E., Mitchell, E.A., Morais, L., Porfirio-Sousa, A.L., Ribeiro, G.M., Tice, A.K., Pánek, T., Kang, S. and Brown, M.W., (2019). Phylogenomics and morphological reconstruction of Arcellinida testate amoebae highlight diversity of microbial eukaryotes in the Neoproterozoic. *Current Biology*, *29*, 6, 991-1001. https://doi.org/10.1016/j.cub.2019.01.078

Lee, Y.C., Chiang, C.C., Huang, P.Y., Chung, C.Y., Huang, T.D., Wang, C.C., Chen, C.I., Chang, R.S., Liao, C.H., and Reisz, R.R., (2017). Evidence of preserved collagen in an Early Jurassic sauropodomorph dinosaur revealed by synchrotron FTIR microspectroscopy. *Nature Communications*, *8,* 14220. https://doi.org/10.1038/ncomms14220.

Lillis, P. G., (2016). The Chuar petroleum system, Arizona and Utah. *Hydrocarbon Source Rocks in Unconventional Plays, Rocky Mountain Region: Denver, Colorado, Rocky Mountain Association of Geologists*, 79-137. https://www.researchgate.net/profile/Paul-Lillis/publication/309313485_The_Chuar_Petroleum_System_Arizona_and_Utah/links/584c5f4208aecb6bd8c2e459/The-Chuar-Petroleum-System-Arizona-and-Utah.pdf

Martí Mus, M., and Moczydłowska, M., (2000). Internal morphology and taphonomic history of the Neoproterozoic vase-shaped microfossils from the

Visingsö Group, Sweden. *Norsk Geologisk Tidsskrift, 8*0, 213–228. https://doi.org/10.1080/002919600433751

Martí Mus, M., Moczydłowska, M. and Knoll, A.H., (2020). Morphologically diverse vase-shaped microfossils from the Russøya Member, Elbobreen Formation, in Spitsbergen. *Precambrian Research*, *350*, 105899. https://doi.org/10.1016/j.precamres.2020.105899

McNamara, M.E., van Dongen, B.E., Lockyer, N.P., Bull, I.D. and Orr, P.J., (2016). Fossilization of melanosomes via sulfurization. *Palaeontology*, *59*, 3, 337-350. https://doi.org/10.1111/pala.12238

Melendez, I., Grice, K., Trinajstic, K., Ladjavardi, M., Greenwood, P. and Thompson, K., (2013). Biomarkers reveal the role of photic zone euxinia in exceptional fossil preservation: An organic geochemical perspective. *Geology*, *41*, 2, 123-126. https://doi.org/10.1130/G33492.1

Morais, L., Fairchild, T. R., Lahr, D. J., Rudnitzki, I. D., Schopf, J. W., Garcia, A. K., and Romero, G. R., (2017). Carbonaceous and siliceous Neoproterozoic vase-shaped microfossils (Urucum Formation, Brazil) and the question of early protistan biomineralization. *Journal of Paleontology*, *91*, 3, 393-406. https://doi.org/10.1017/jpa.2017.16

Myers, C.E., Bergmann, K.D., Sun, C.Y., Boekelheide, N., Knoll, A.H. and Gilbert, P.U., (2018). Exceptional preservation of organic matrix and shell microstructure in a Late Cretaceous Pinna fossil revealed by photoemission electron spectromicroscopy. *Geology*, *46*, 8, 711-714. https://doi.org/10.1130/G45271.1

Ogden, C.G., (1984). Shell structure of some testate amoebae from Britain (Protozoa, Rhizopoda). *Journal of Natural History*, *18*, 3, 341-361. https://doi.org/10.1080/00222938400770291

Porter, S.M., and Knoll, A.H., (2000). Testate amoebae in the Neoproterozoic Era: evidence from vase-shaped microfossils in the Chuar Group, Grand Canyon. *Paleobiology*, *26*, 3, 360-385. https://doi.org/10.1666/0094-8373(2000)026%3C0360:TAITNE%3E2.0.CO;2

Porter, S. M., Meisterfeld, R., and Knoll, A. H., (2003). Vase-shaped microfossils from the Neoproterozoic Chuar Group, Grand Canyon: a classification guided by modern testate amoebae. *Journal of Paleontology*, *77*, 3, 409-429. https://doi.org/10.1666/0022-3360(2003)077%3C0409:VMFTNC%3E2.0.CO;2

Porter, S.M., and Riedman, L.A., (2016). Systematics of organic-walled microfossils from the mid-Neoproterozoic Chuar Group, Grand Canyon, Arizona: *Journal of Paleontology*, *90*, 815–853. https://doi.org/10.1017/jpa.2016.57

Porter, S.M., and Riedman, L.A., (2019). Evolution: Ancient Fossilized Amoebae Find Their Home in the Tree. *Current Biology*, *29*, 6, R212-R215. https://doi.org/10.1016/j.cub.2019.02.003

Raven, M.R., Fike, D.A., Gomes, M.L., Webb, S.M., Bradley, A.S. and McClelland, H.L.O., (2018). Organic carbon burial during OAE2 driven by changes in the locus of organic matter sulfurization. *Nature Communications*, *9,* 1, 1-9. https://doi.org/10.1038/s41467-018-05943-6

Raven, M.R., Keil, R.G. and Webb, S.M., (2021). Microbial sulfate reduction and organic sulfur formation in sinking marine particles. *Science*, *371*, 6525, 178-181. https://doi.org/10.1126/science.abc6035

Rasmussen, B. and Muhling, J.R., (2019). Organic-rich microfossils produced by oil infiltration of hollow silicified bacteria: Evidence from the ca. 340 Ma Red Dog Zn-Pb deposit, Alaska. *Geology*, *47*, 1107-1111. https://doi.org/10.1130/G46346.1

Rasmussen, B., Muhling, J.R. and Fischer, W.W., (2021). Ancient Oil as a Source of Carbonaceous Matter in 1.88-Billion-Year-Old Gunflint Stromatolites and Microfossils. *Astrobiology*, *21*, 9, 1-18. https://doi.org/10.1089/ast.2020.2376

Riedman, L. A., Porter, S. M., and Calver, C. R., (2018). Vase-shaped microfossil biostratigraphy with new data from Tasmania, Svalbard, Greenland, Sweden and the Yukon. *Precambrian Research*, *319*, 19-36. https://doi.org/10.1016/j.precamres.2017.09.019

Rooney, A.D., Austermann, J., Smith, E.F., Li, Y., Selby, D., Dehler, C.M., Schmitz, M.D., Karlstrom, K.E. and Macdonald, F.A., (2018). Coupled Re-Os and U-Pb geochronology of the Tonian Chuar Group, Grand Canyon. *GSA Bulletin*, *130*, 1085-1098. https://doi.org/10.1130/B31768.1

Schiffbauer, J.D., Xiao, S., Cai, Y., Wallace, A.F., Hua, H., Hunter, J., Xu, H., Peng, Y. and Kaufman, A.J., (2014). A unifying model for Neoproterozoic–Palaeozoic exceptional fossil preservation through pyritization and carbonaceous compression. *Nature Communications*, *5*, 1, 1-12. https://doi.org/10.1038/ncomms6754

Sergeev, V.N., Schopf, J.W., (2010). Taxonomy, paleoecology and biostratigraphy of the late Neoproterozoic Chichkan microbiota of south Kazakhstan: the marine biosphere on the eve of metazoan radiation. *Journal of Paleontology, 84,* 3, 363–401. https://doi.org/10.1666/09-133.1

Sinninghe Damsté, J.S. and De Leeuw, J.W., (1987). The origin and fate of isoprenoid C20 and C15 sulphur compounds in sediments and oils. *International Journal of Environmental Analytical Chemistry*, *28*, 1-19. https://doi.org/10.1080/03067318708078398

Sinninghe Damsté, J.S. and De Leeuw, J.W., (1990). Analysis, structure and geochemical significance of organically-bound sulphur in the geosphere: state of the art and future research. *Organic Geochemistry*, *16*, 1077-1101. https://doi.org/10.1016/0146-6380(90)90145-P

Strauss, J. V., Rooney, A. D., Macdonald, F. A., Brandon, A. D., & Knoll, A. H., (2014). 740 Ma vase-shaped microfossils from Yukon, Canada: Implications for Neoproterozoic chronology and biostratigraphy. *Geology*, *42*, 8, 659-662. https://doi.org/10.1130/G35736.1

Summons, R. E., Brassell, S. C., Eglinton G., Evans, E., Horodyski, R.J., Robinson, N., and Ward D.M., (1988). Distinctive hydrocarbon biomarkers from fossiliferous sediment of the Late Proterozoic Walcott Member, Chuar Group, Grand Canyon, Arizona. *Geochimica et Cosmochimica Acta, 52*, 2625–2637. https://doi.org/10.1016/0016-7037(88)90031-2

Timmons, J.M., Karlstrom, K.E., Dehler, C.M., Geissman, J.W. and Heizler, M.T., (2001). Proterozoic multistage (ca. 1.1 and 0.8 Ga) extension recorded in the Grand Canyon Supergroup and establishment of northwest-and north-trending tectonic grains in the southwestern United States. *GSA Bulletin*, *113,* 2, 163-181. https://doi.org/10.1130/0016-7606(2001)113<0163:PMCAGE>2.0.CO;2

Timmons, J.M., Karlstrom, K.E., Heizler, M.T., Bowring, S.A., Gehrels, G.E., and Crossey, L.J., (2005). Tectonic inferences from the ca. 1255–1100 Ma Unkar Group and Nankoweap Formation, Grand Canyon: Intracratonic deformation and basin formation during protracted Grenville orogenesis. *GSA Bulletin*, *117*,11-12, 1573–1595. https://doi.org/10.1130/B25538.1

Vidal, G., (1979). Acritarchs from the upper Proterozoic and lower Cambrian of East Greenland. *Grønlands Geologiske Undersøgelse*, *134*. http://pascal-francis.inist.fr/vibad/index.php?action=getRecordDetail&idt=PASCALGEODEBRGM8020289287

Walcott, C. D. (1899). Precambrian fossiliferous formations. *Geological Society of America Bulletin, 10*, 199–244. https://doi.org/10.1130/GSAB-10-199

Werne, J.P., Hollander, D.J., Lyons, T.W. and Damsté, J.S.S., (2004). Organic sulfur biogeochemistry: recent advances and future research directions. *Geological Society of America Special Papers*, *379*, 135-150. https://doi.org/10.1130/0-8137-2379-5.135

Werne, J.P., Lyons, T.W., Hollander, D.J., Schouten, S., Hopmans, E.C. and Damsté, J.S.S., (2008). Investigating pathways of diagenetic organic matter sulfurization using compound-specific sulfur isotope analysis. *Geochimica et Cosmochimica Acta*, *72,* 14, 3489-3502. https://doi.org/10.1016/j.gca.2008.04.033

Woltz, C.R., Porter, S.M., Agić, H., Dehler, C.M., Junium, C.K., Riedman, L.A., Hodgskiss, M.S.W., Wörndle, S. and Halverson, G.P., (2021), Total organic carbon and the preservation of organic-walled microfossils in Precambrian shale. *Geology*, *49*, 556-560. https://doi.org/10.1130/G48116.1

Xiao, S., Shen, B., Tang, Q., Kaufman, A.J., Yuan, X., Li, J. and Qian, M., (2014). Biostratigraphic and chemostratigraphic constraints on the age of early Neoproterozoic carbonate successions in North China. *Precambrian Research*, *246*, 208-225. https://doi.org/10.1016/j.precamres.2014.03.004

Zolotov, M.Y. and Shock, E.L., (2005). Formation of jarosite-bearing deposits through aqueous oxidation of pyrite at Meridiani Planum, Mars. *Geophysical Research Letters*, *32*, 21, L21203. https://doi.org/10.1029/2005GL024253

Zumberge, J. A., Rocher, D., & Love, G. D., (2019). Free and kerogen-bound biomarkers from late Tonian sedimentary rocks record abundant eukaryotes in mid-Neoproterozoic marine communities. *Geobiology*, *18*, 3, p. 326-347. https://doi.org/10.1111/gbi.12378

Appendix

Figure S1: Energy-dispersive spectroscopy (EDS) spot analyses of VSM material from sample CS2. The thin section is coated in Au, Pd. The reference image is BSE. (CS2.1)

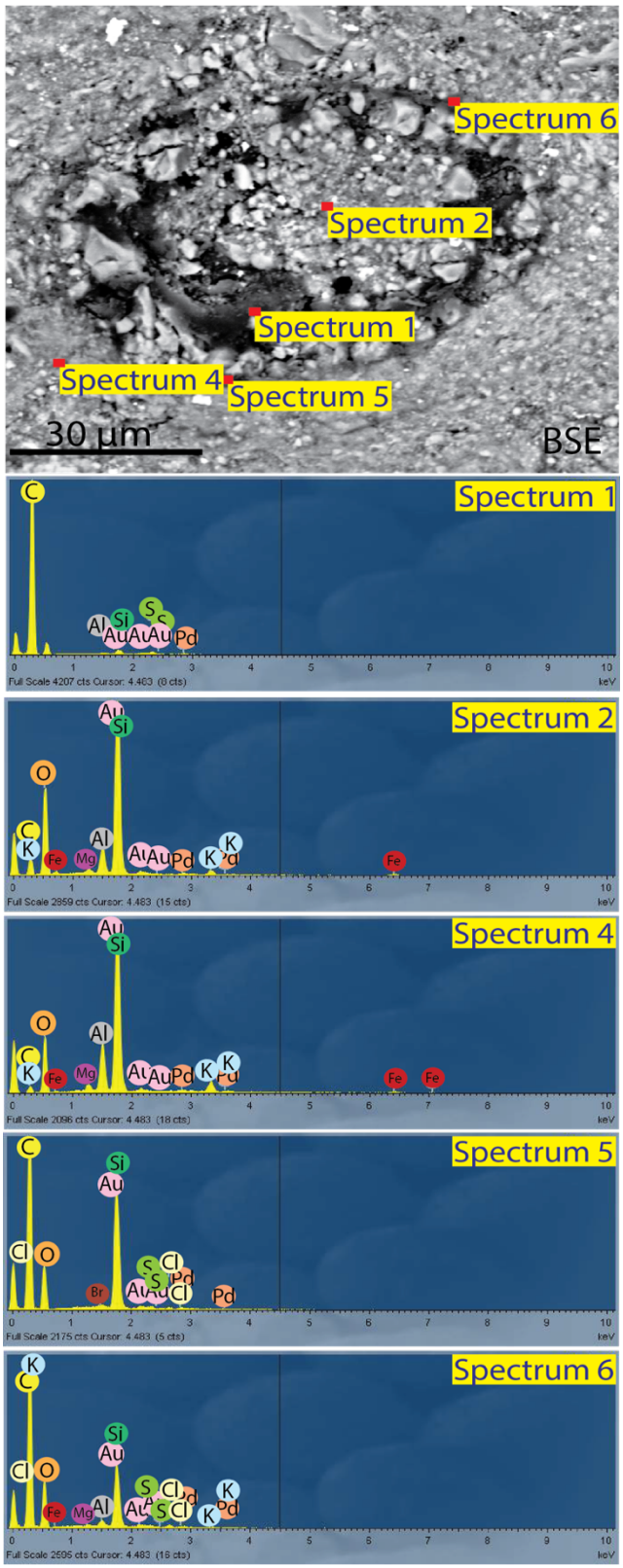

Figure S2: Energy-dispersive spectroscopy (EDS) spot analyses of VSM material from sample CS3. The thin section is coated in Au, Pd. The reference image is BSE. (CS3.3)

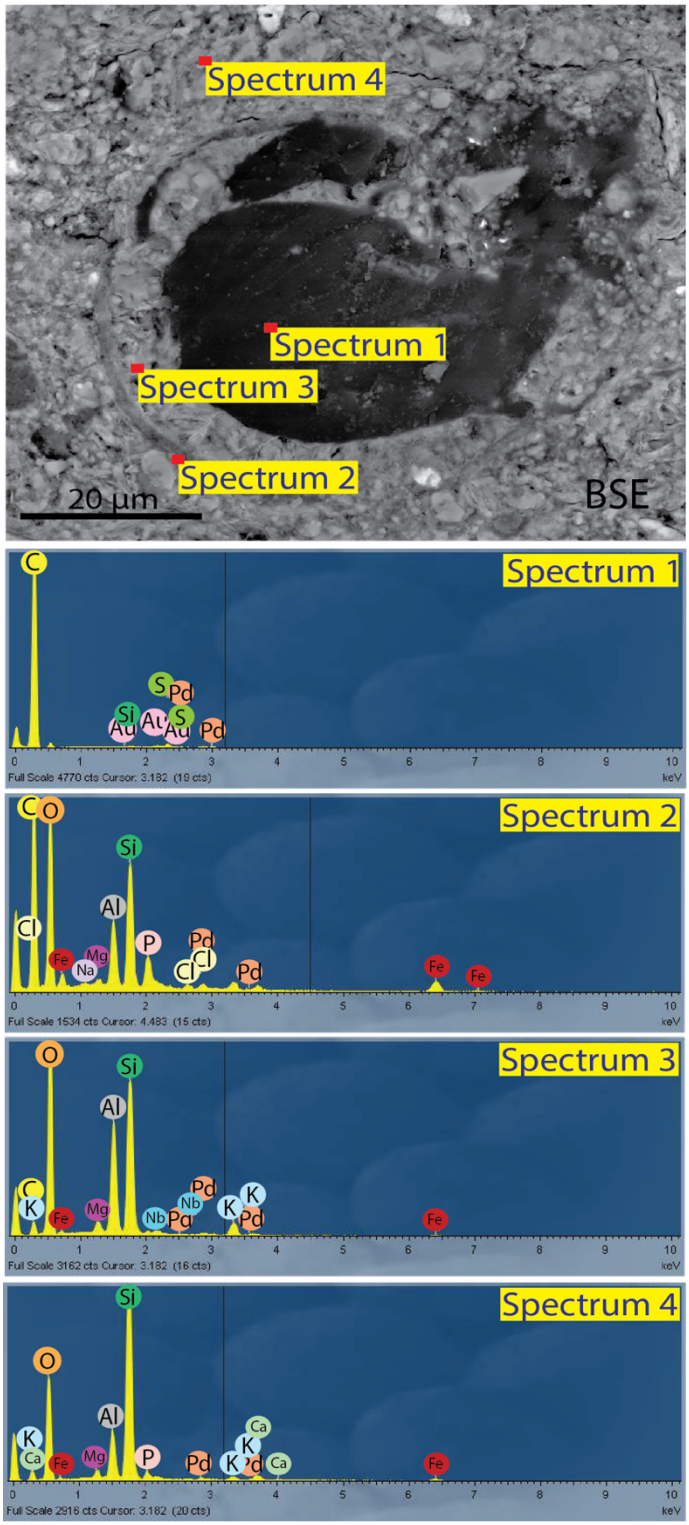

Figure S3: Energy-dispersive spectroscopy (EDS) spot analyses of VSM material from sample CS3. The thin section is coated in Au, Pd. The reference image is BSE. (CS3.3)

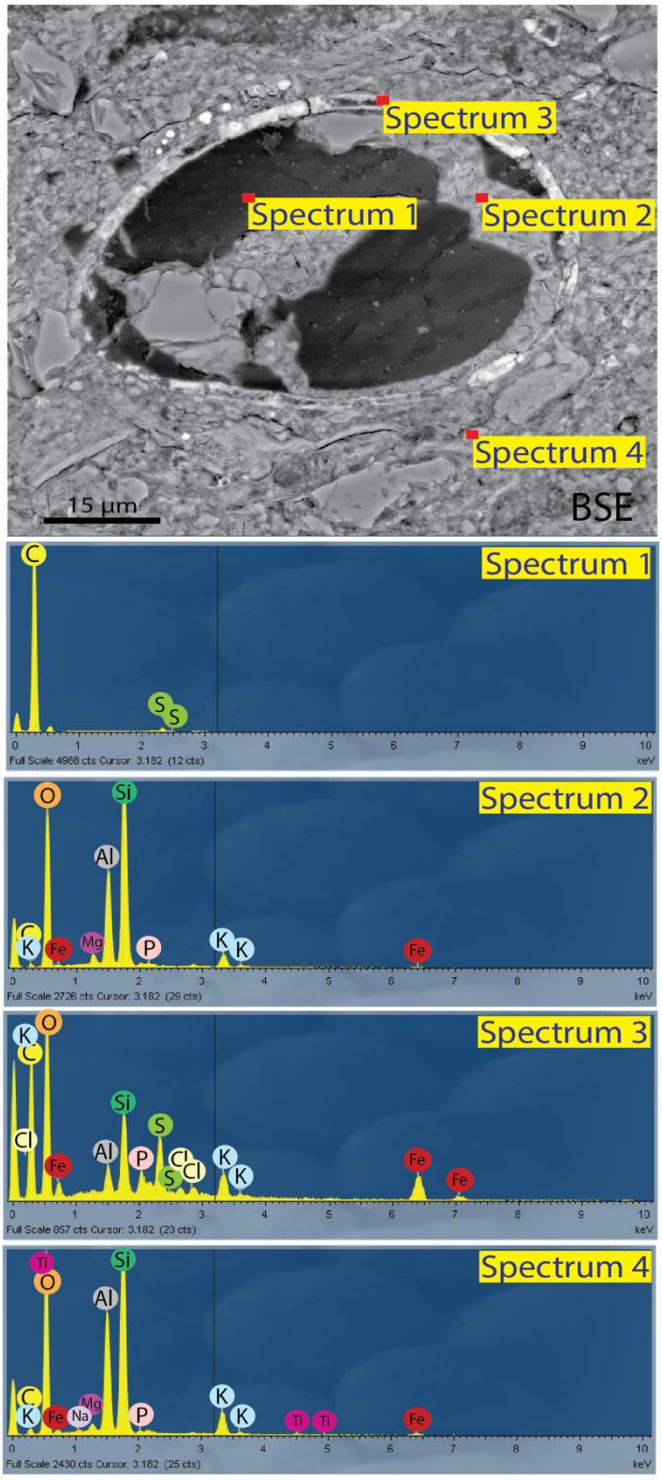

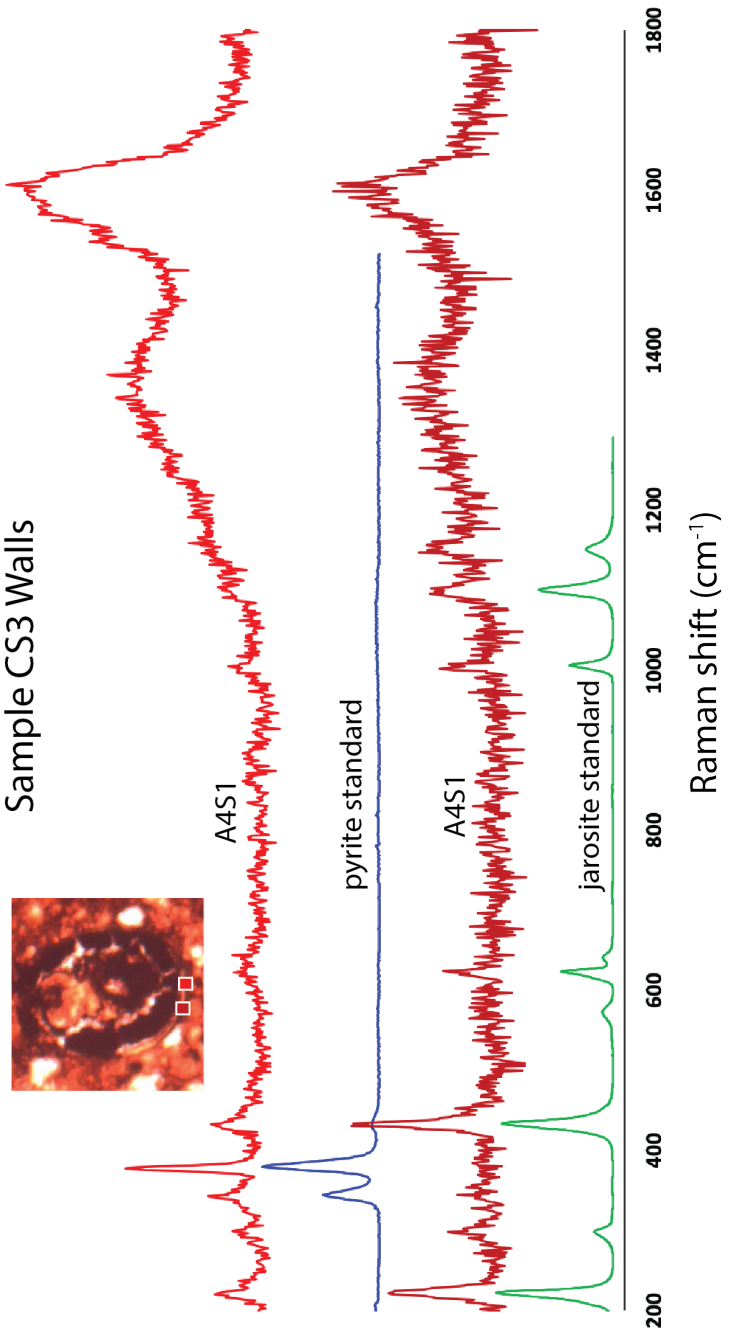

Figure S4. Raman spectra of walls of a VSM from sample CS3, pictured here in optical microscopy and in Figure 9K, plotted together with pyrite and jarosite standards. (CS3.1)

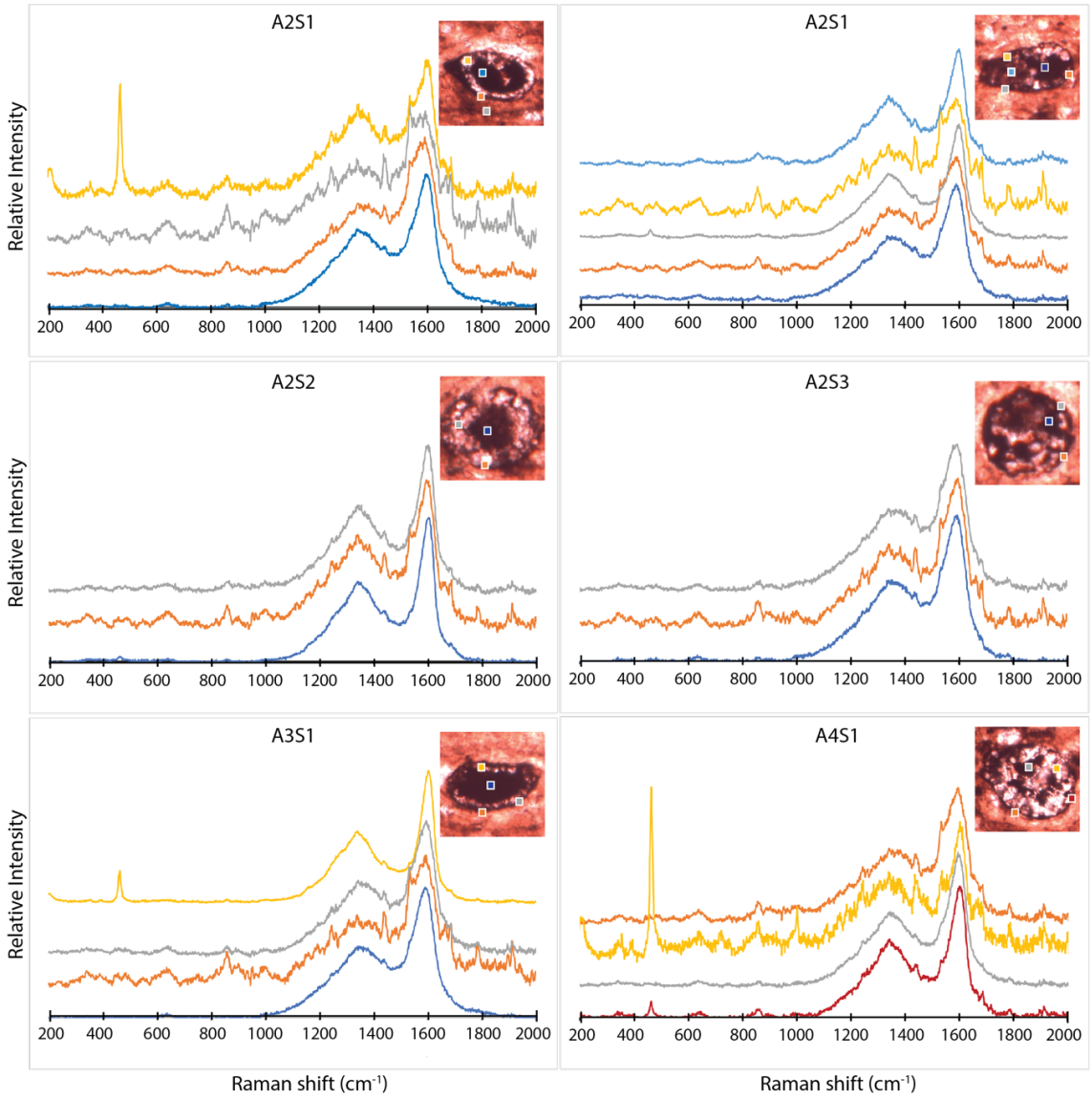

Figure S5. All reported baseline subtracted Raman spectra of VSMs of sample CS2

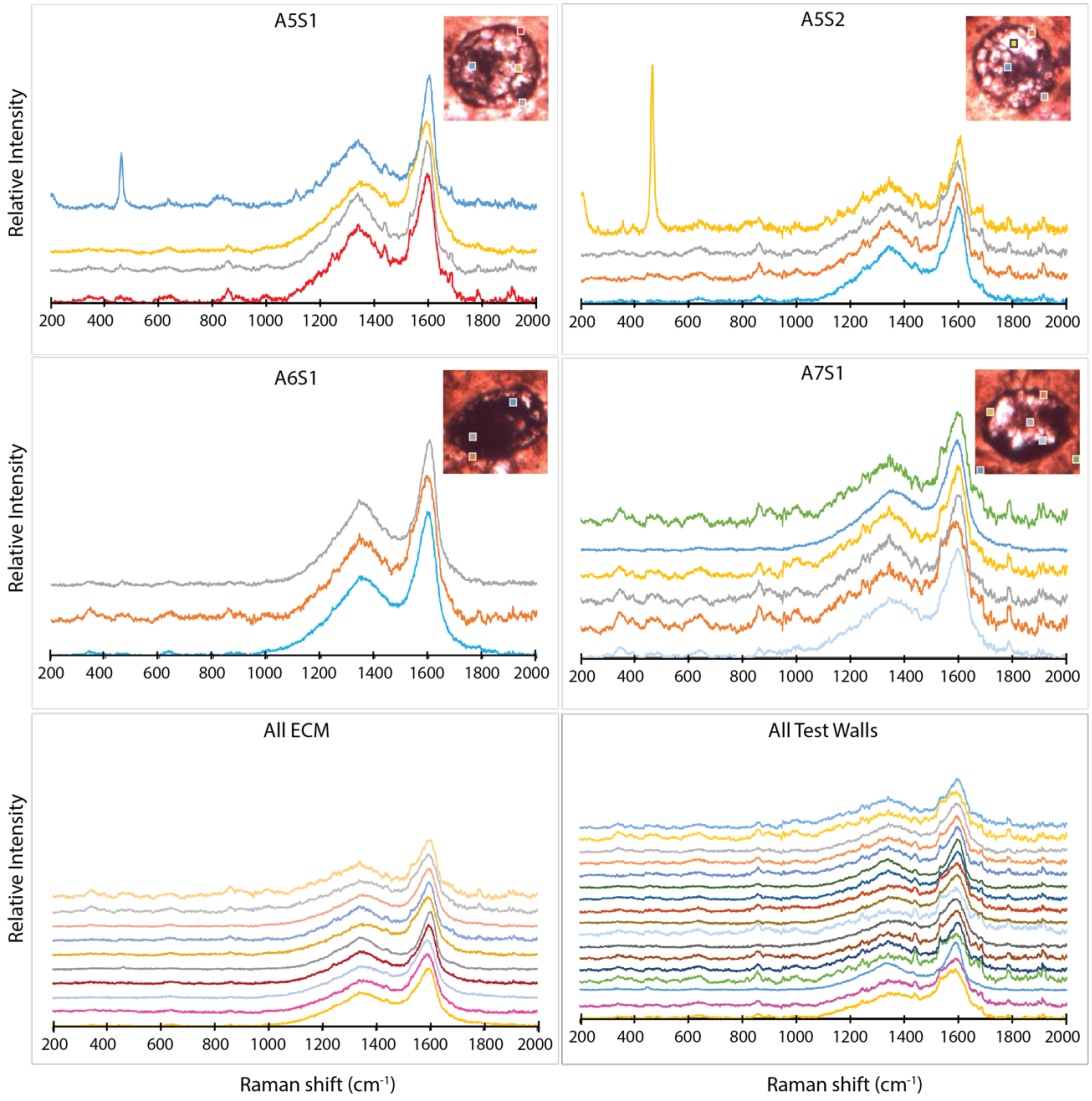

Figure S5 continued

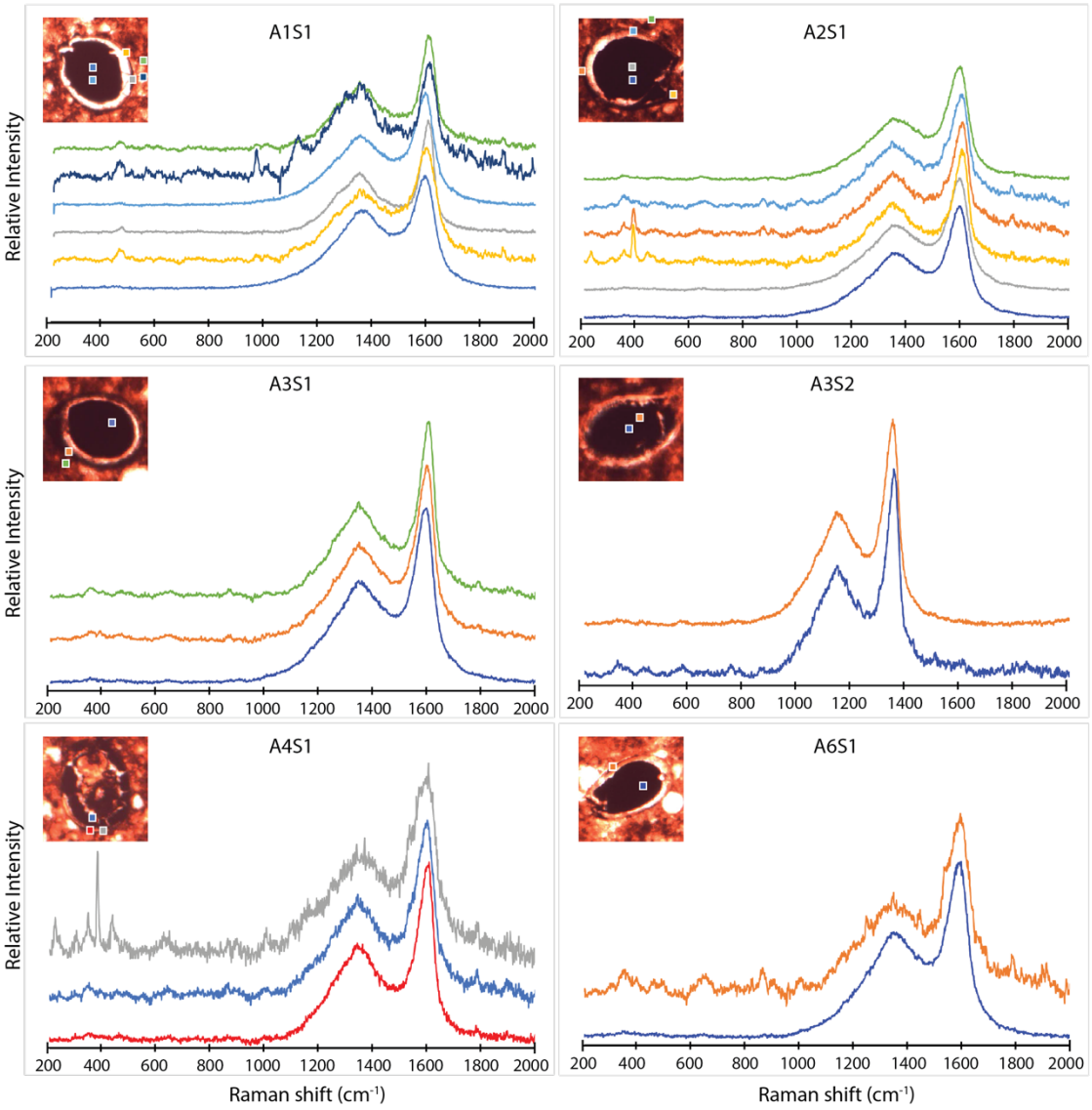

Figure S6. All reported baseline subtracted Raman spectra of VSMs of sample CS3

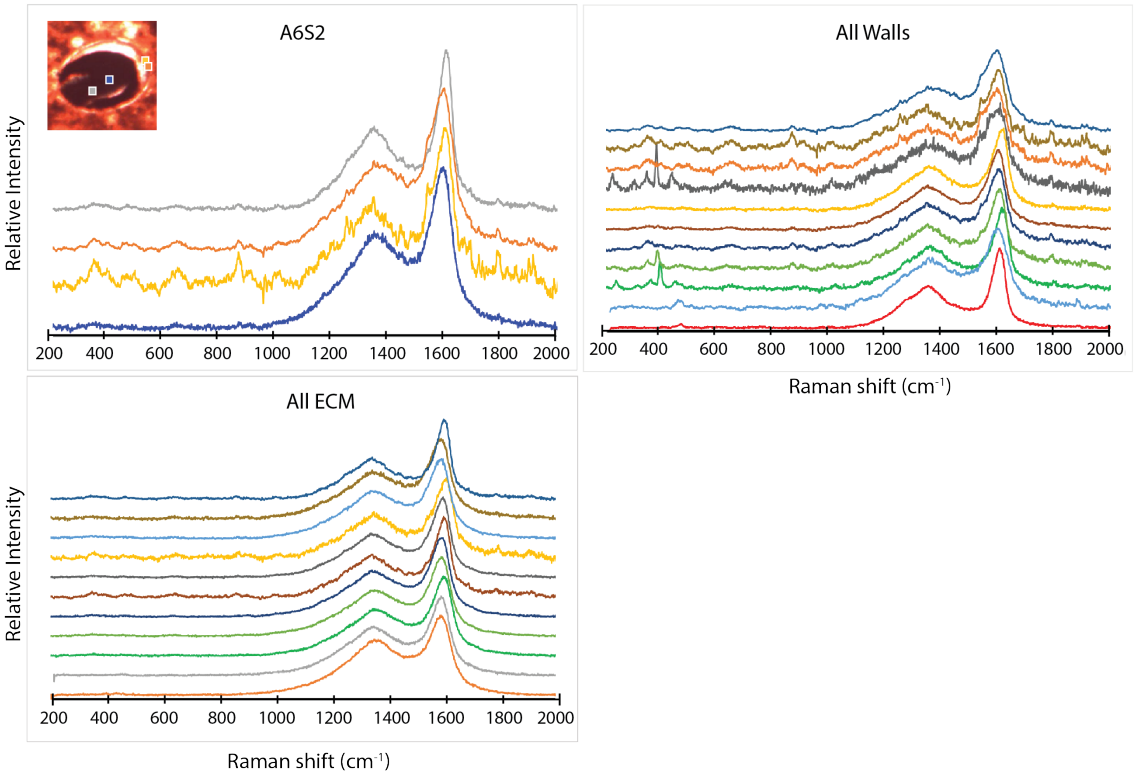

Figure S6 continued

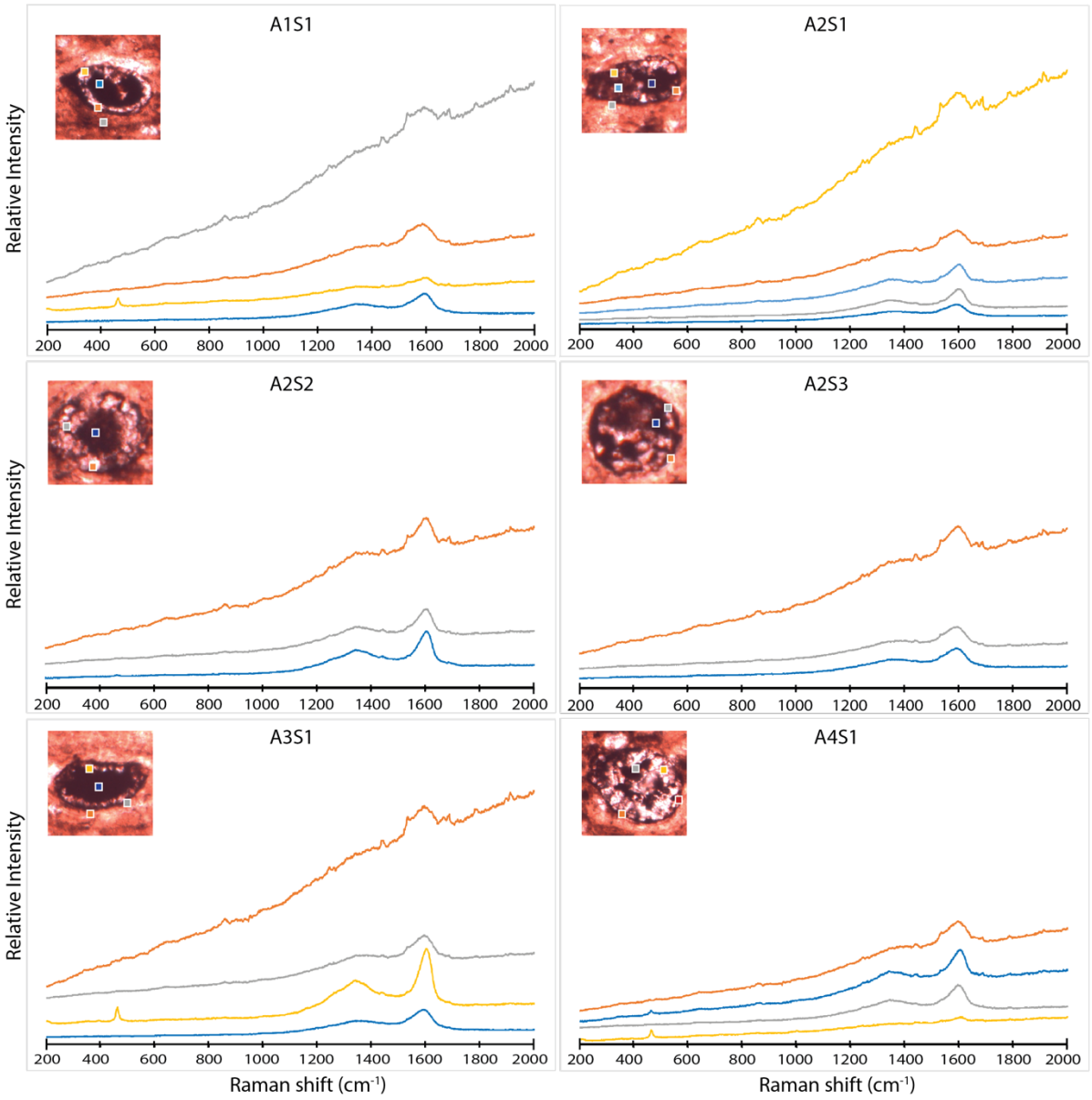

Figure S7. All reported raw Raman spectra of VSMs of sample CS2

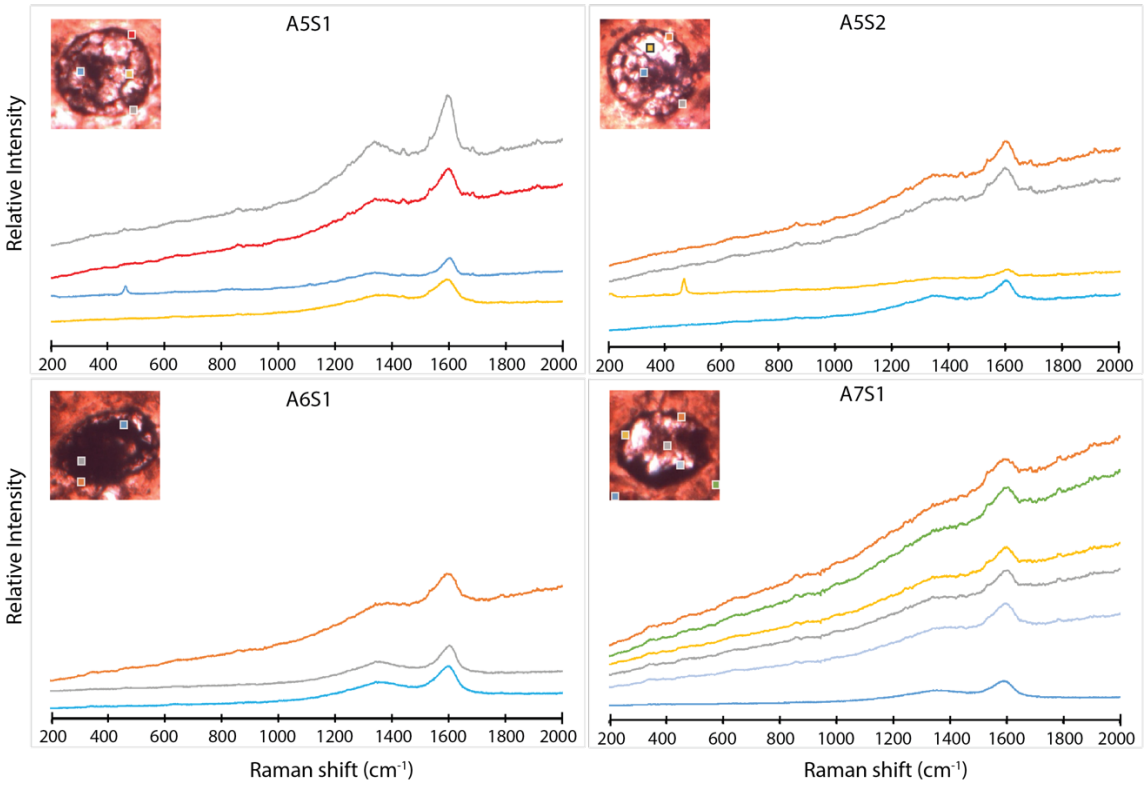

Figure S7 continued

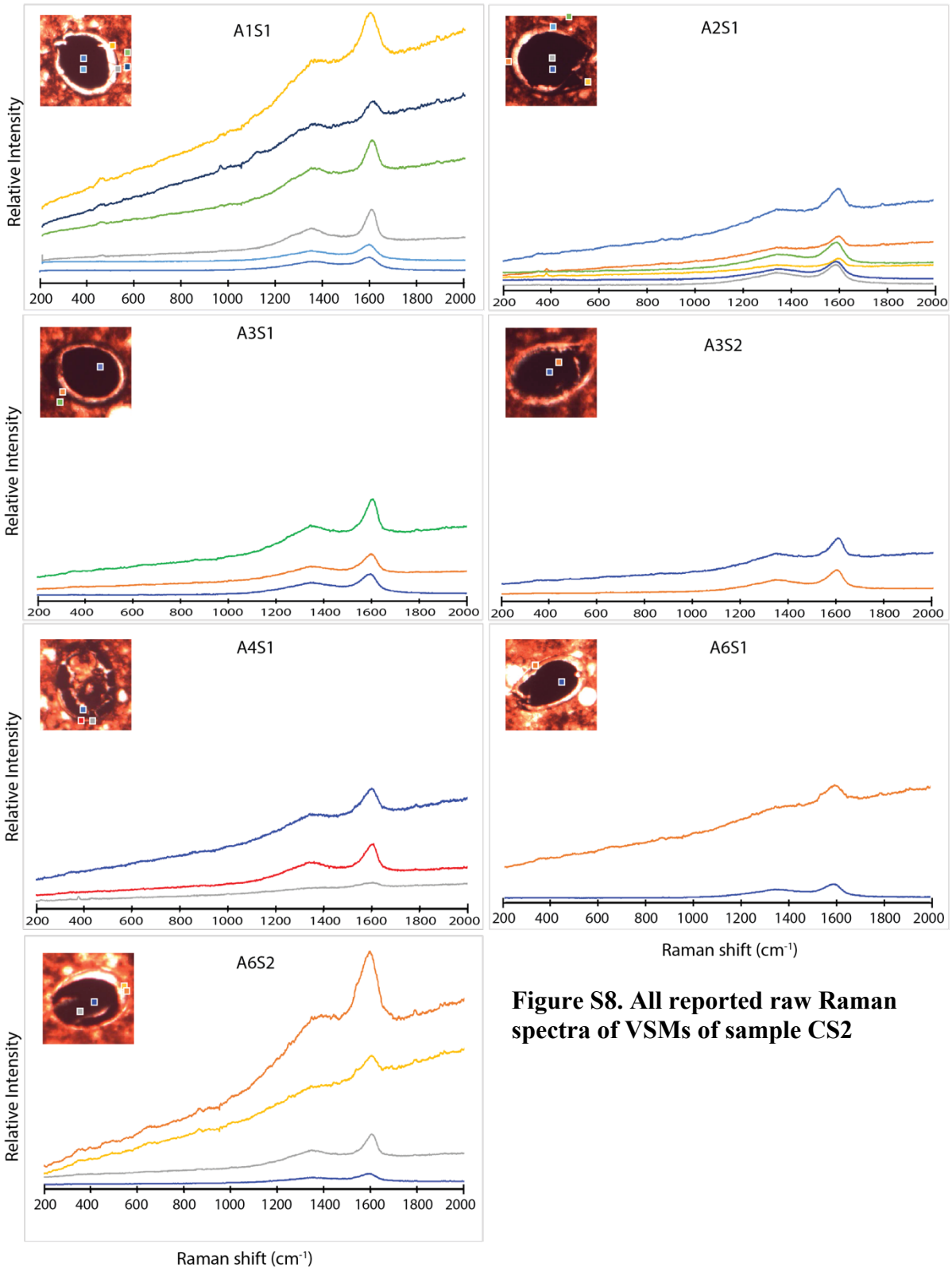

Figure S8. All reported raw Raman spectra of VSMs of sample CS2